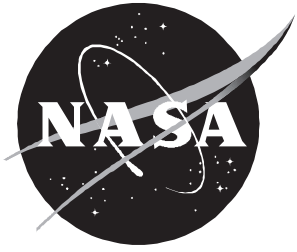


# Lifetimes of Lunar Satellite Orbits

---

*Kurt W. Meyer, James J. Buglia, and Prasun N. Desai*



# Lifetimes of Lunar Satellite Orbits

---

*Kurt W. Meyer*  
*The George Washington University/JIAFS • Washington, D.C.*

*James J. Buglia*  
*Flight Mechanics & Control, Inc. • Hampton, Virginia*

*Prasun N. Desai*  
*Langley Research Center • Hampton, Virginia*

National Aeronautics and  
Space Administration  
Code JTT  
Washington, D.C.  
20546-0001

B U L K R A T E
POSTAGE & FEES PAID
NASA Permit No. G-27

*Official Business*  
*Penalty for Private Use, \$300*

*Postmaster: If undeliverable (Section 158 Postal Manual) Do Not Return*

---

## Acknowledgments

This technical report is the culmination of research in the Vehicle Analysis Branch of the Space Systems Division at Langley Research Center, during which time the authors received technical guidance from numerous sources. We particularly wish to express appreciation to Dr. Gerald Walberg of North Carolina State University at Raleigh for providing valuable assistance in developing a plan of action for addressing lunar parking orbit issues. Additionally, we would also like to thank Robert Tolson of The George Washington University for sharing his insight on modeling the Moon's gravitational field, and Wayne McClain of Draper Laboratories and Richard Cook of the Jet Propulsion Laboratory for their comments and suggestions.

## Summary

Lifetimes of low-altitude lunar orbits are studied in this report to identify feasible parking orbits for future lunar missions. The lunar missions currently under study, unlike the Apollo missions, involve long stay times. To determine orbital lifetimes of lunar parking orbits, a model to describe the nonspherical mass distribution of the Moon must be adopted. A short discussion of previous attempts to describe the Moon's gravitational field is included, and emphasis is placed on spherical harmonic-gravity models. A subset of the fifth-order and fifth-degree lunar gravity model was adopted in this investigation to generate orbital lifetime predictions. This simplified model consists of the five gravitational coefficients  $J_2$ ,  $J_3$ ,  $J_5$ ,  $C_{22}$ , and  $C_{31}$ .

The primary perturbation on a low-altitude (100 km or 300 km) lunar parking orbit is the Moon's nonspherical gravity field. In this analysis, all other perturbations (third body perturbations, solar radiation pressure, etc.) are neglected. Although perturbations due to the Earth and the Sun are not negligible for lunar orbits, these effects are small compared with the Moon's nonspherical potential for all the orbits considered in this analysis. By investigating the effects that initial conditions have on the subsequent lifetime of an orbit, a technique is introduced to aid mission planners in the selection of lunar parking orbits. In this investigation, the lifetimes of near-circular parking orbits, with various initial orbital elements and either 100-km or 300-km perilune altitude, are analyzed for mission planning purposes.

Orbital lifetimes are heavily dependent on the initial conditions of the orbit, particularly the initial inclination and argument of perilune. The lunar gravity model utilized in this analysis for the 100-km initial perilune altitude case yields lifetime predictions of less than 40 days for some orbits, and more than a year for others. Five distinct bands of short-lifetime orbits appear as a function of the initial inclination; these bands are separated by bands of long-lifetime orbits. Of particular interest is a set of orbits with an inclination of approximately  $70^\circ$ ; this set of orbits yields long lifetimes and provides the high latitude coverage that is desirable for various missions. The  $J_5$  coefficient contributes the dominant effect in perilune altitude decay and, therefore, orbital lifetimes.

The methods presented in this report are suitable for incorporating the Moon's nonspherical gravitational effects into the preliminary design level for future lunar mission planning. However, inconsistencies and limitations, caused primarily by a lack of

satellite tracking data from the far side of the Moon, are inherent in all existing lunar gravity models. The uncertainty in orbital lifetime predictions due to errors in the lunar gravity model is addressed through the use of sensitivity coefficients. The uncertainty in the rate of perilune altitude decay that corresponds to the uncertainty in the values of the coefficients for the gravity model adopted in this analysis is presented. Also, plots of the values of the sensitivity coefficients, which can be used to evaluate the uncertainty in perilune-altitude decay rates of each gravitational coefficient for any lunar gravity model, are presented.

## Introduction

President Bush's proposal of a Space Exploration Initiative in 1989 sparked a renewed interest in lunar mission planning. The objectives outlined in this initiative include the establishment of a permanent lunar outpost. (See refs. 1 and 2.) Lunar stay times on the order of 30 to 180 days will be required for initial deployment and ongoing support of the outpost. In some analyses, preliminary missions will involve the insertion of a satellite into a low-altitude lunar orbit to map the Moon's surface. Also in these analyses, initial manned missions will require the placement of a lunar transfer vehicle in a low-altitude parking orbit. Ongoing support of an outpost might include the placement of a space station in low lunar orbit. Any of these missions will require spacecraft to be in lunar parking orbits for long periods of time. Previous orbital determination studies for lunar satellites have indicated that the Moon's nonspherical gravity field will have a great effect on the subsequent lifetime of the orbit. (See refs. 3 to 5.) In fact, a lunar-orbit space station proposed by NASA to be in a 60-n.mi. (111 km) circular polar orbit about the Moon was found to impact the lunar surface in 140 days if no station-keeping altitude boost maneuvers were performed. (See ref. 6.)

An important element involved in establishing a base on the Moon is the initial manned mission to the lunar surface. As with the Apollo missions, the lunar transfer vehicle (LTV) will be inserted into a parking orbit about the Moon at arrival. Apollo missions restricted these parking orbits to circular, near-equatorial orbits. However, the utilization of parking orbits at all inclinations must be addressed to accommodate the vast array of lunar missions currently being proposed. The LTV will remain in this parking orbit until a departure burn for return to Earth is initiated. The transfer of cargo and personnel to the lunar surface is accomplished by the descent of a lunar lander from the parking orbit. Ascent

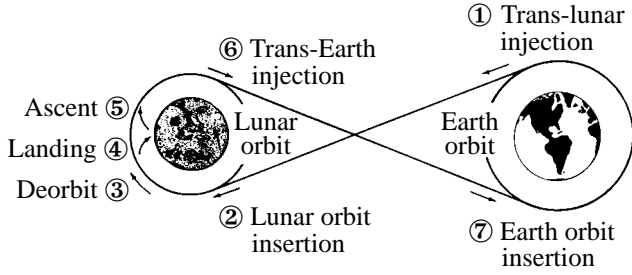


Figure 1. Earth-lunar mission sequence. (From ref. 1.)

and rendezvous of the lander with the LTV in the parking orbit initiates the Earth-return sequence of the mission. (See fig. 1.) Therefore, long stay times on the lunar surface will require that the LTV remain in a parking orbit for a long period. The mission designer must address the variations in the orientation of the parking orbit for the duration of the mission to establish the necessary  $\Delta V$  requirements for performing the rendezvous and trans-Earth injection maneuvers.

Since the Apollo missions involved only short stay times at the Moon (on the order of 1 to 3 days), little work was performed on predicting long term changes in the parking orbits of lunar modules. However, for longer stay times (30 to 180 days), an accurate model of the Moon's gravity field is required for preliminary mission planning, especially with low-altitude parking orbits. The need for long orbital lifetimes is a key criterion in the process of selecting feasible parking orbits. By investigating the effects that initial conditions have on the subsequent lifetime of an orbit, a technique is introduced that will aid mission planners in the selection of lunar parking orbits.

Because of the Moon's irregular internal structure and surface shape, the lifetime of a lunar satellite orbit is constrained by the nonspherical nature of the Moon's gravity field. In the present analysis, a simplified gravitational model of the Moon is introduced that will enable mission planners to easily predict long-term changes in lunar parking orbits at the preliminary design level. The development of a simplified gravitational model with sufficient accuracy is necessary to investigate orbital lifetimes for the large number of initial orbital parameters possible. Utilization of a simplified model will significantly reduce the required computational time needed to perform this analysis. The effect of individual terms in gravity models on orbital lifetimes is also addressed. By investigating the effects of the lunar gravity model on the various parking orbits, the parameters that are most important in determining lifetime predictions are identified.

## Nomenclature

$A_{nm}, B_{nm}$	Fourier coefficients
$a$	semimajor axis, km
$C_{nm}, S_{nm}$	gravitational coefficients
$dm$	infinitesimal mass element, kg
$e$	eccentricity
$\bar{e}$	eccentricity averaged over period of third body about central body
$e_{\text{new}}$	new value of eccentricity (after integration)
$e_{\text{old}}$	old value of eccentricity (before integration)
$G$	gravitational constant, $6.67 \times 10^{-11} \text{ m}^3\text{-kg}^{-1}\text{-s}^{-2}$
$h$	altitude, km
$i$	inclination, deg
$\bar{i}$	inclination averaged over period of third body about central body, deg
$J_n$	zonal gravitational coefficient, $-C_{n0}$
LTV	lunar transfer vehicle
$M$	mean anomaly, deg
$\mathcal{M}$	mass of Moon, $7.35 \times 10^{22} \text{ kg}$
$n$	mean angular motion, rad/day
$\bar{n}$	mean angular motion averaged over period of third body about central body, rad/day
$n_3$	mean angular motion of third body about central body, rad/day
$P_{nm}$	associated Legendre polynomial
$\mathbf{P}$	position vector
$R$	radius of Moon, 1739 km
$\mathcal{R}$	distance between mass element and exterior point, km
$r$	radius, km
$\dot{r}$	rate of altitude decay, km/day
$t$	time, days
$\Delta t$	integration time step, 1 day
$U$	gravitational potential
$\nabla U$	gradient of gravitational potential

$V$	disturbing function (nonspherical gravitational potential)
$\Delta V$	velocity increment, m/sec
$\mathcal{V}$	volume, km <sup>3</sup>
$w$	rotation rate of Moon, 13-18°/day
$x, y, z$	position in Cartesian coordinates, km
$\dot{x}, \dot{y}, \dot{z}$	velocity in Cartesian coordinates, km/sec
$\lambda$	longitude, deg
$\nu$	true anomaly, deg
$\rho$	density, g/cm <sup>3</sup>
$\sigma_{C_{nm}}$	standard deviation of gravitational coefficient
$\sigma_{\dot{r}_p}$	variance in perilune altitude decay rate, km/day
$\phi$	latitude, deg
$\Omega$	longitude of ascending node, deg
$\Omega_i$	inertial node longitude, deg
$\Omega_s$	selenographic node longitude, deg
$\left(\frac{d\Omega}{dt}\right)_{31}$	$\frac{d\Omega}{dt}$ contribution for $C_{31}$ term
$\omega$	argument of perilune, deg
$\bar{\omega}$	argument of perilune averaged over period of third body about central body, deg
Subscripts:	
$m$	order of gravitational coefficient
$n$	degree of gravitational coefficient
$p$	perilune

## Background

### Gravitational Potential Theory and Resulting Perturbations

To determine the orbital lifetime of a satellite, the gravitational field of the attracting body must first be described. Since gravity is a conservative force, the gravitational field of a body can be represented by a potential function. A solution for the form of the potential of a body can be obtained in terms of a mass integral definition or by finding a solution to Laplace's equation. In the first approach (refs. 7 and 8), infinitesimal mass elements are integrated over the entire body to describe the potential at

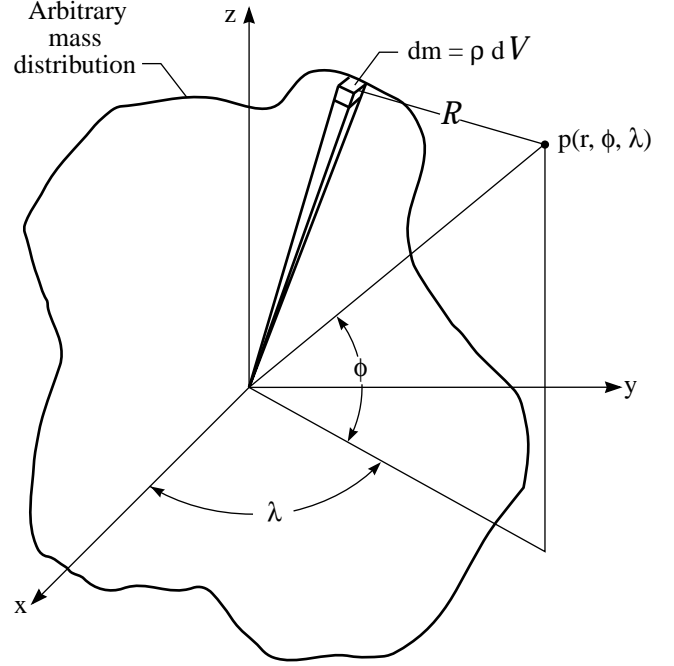


Figure 2. Solution for potential of a body using a mass integral definition.

an exterior point,  $p(r, \phi, \lambda)$ , where  $r$  is the radial distance between the point and the origin, and  $\phi$  and  $\lambda$  are the latitude and longitude of the point (fig. 2) as follows:

$$\begin{aligned}
 U(r, \phi, \lambda) &= \int_{\text{Body}} dU = G \int_{\text{Body}} \frac{dm}{\mathcal{R}} \\
 &= G \int_{\mathcal{V}_{\text{body}}} \frac{\rho(r, \phi, \lambda) d\mathcal{V}}{\mathcal{R}} \quad (1)
 \end{aligned}$$

where  $\mathcal{R}$  is the distance between the mass element and the exterior point  $p$ ,  $\rho$  is the density function of the body, and  $\mathcal{V}$  is the volume of the body. The  $\frac{1}{\mathcal{R}}$  term is expanded in a Legendre polynomial series, and the addition theorem for Legendre associated polynomials is used to write the potential in the form

$$\begin{aligned}
 U &= \sum_{n=0}^{\infty} \sum_{m=0}^n \left( \frac{R^n}{r^{n+1}} \right) P_{nm}(\sin \phi) \\
 &\quad \times [A_{nm} \cos(m\lambda) + B_{nm} \sin(m\lambda)] \quad (2)
 \end{aligned}$$

This spherical harmonic expansion of the potential function can also be obtained by using a separation-of-variables method to solve Laplace's equation. This approach is outlined in reference 9.

The  $A_{00}$  term represents the uniform spherical potential contribution  $\frac{GM}{r}$ . Assuming that the origin of

the coordinate system is at the center of mass of the body, then  $A_{10} = A_{11} = B_{11} = 0$ . By also introducing the variables  $C_{nm} = \frac{A_{nm}}{GM}$  and  $S_{nm} = \frac{B_{nm}}{GM}$ , the potential can be written in the traditional form as follows:

$$U = \frac{GM}{r} \left\{ 1 + \sum_{n=2}^{\infty} \sum_{m=0}^n \left( \frac{R}{r} \right)^n P_{nm}(\sin \phi) \right. \\ \left. \times [C_{nm} \cos(m\lambda) + S_{nm} \sin(m\lambda)] \right\} \quad (3)$$

If the density function of the body is known, the value of the coefficients  $C_{nm}$  and  $S_{nm}$  can be determined by integration of the appropriate mass integrals over the volume of the body. In practice, since the density function is not known, the values of the  $C_{nm}$  and  $S_{nm}$  coefficients are determined empirically by tracking satellites orbiting the body. Using statistical methods, the best set of  $C_{nm}$  and  $S_{nm}$  coefficients that describe the orbit are determined. (See section ‘‘Lunar Gravity Models.’’)

The disturbing function  $V$ , defined as  $V \equiv U - \frac{GM}{r}$ , contains the nonspherical gravitational contribution to the potential. This nonspherical gravitational contribution arises from the nonspherical mass or density distribution of the body. The net effect of this nonuniformity is the creation of a small disturbance force on an orbiting body; this disturbance causes a change in the orbital elements over time. The Lagrange planetary equations (ref. 10) describe the effects of the disturbing function on an orbiting body as follows (the  $n$  term in eq. (4f) is a result of the  $\frac{GM}{r}$  term):

$$\frac{da}{dt} = \frac{2}{na} \left( \frac{\partial V}{\partial M} \right) \quad (4a)$$

$$\frac{de}{dt} = \frac{1 - e^2}{na^2 e} \frac{\partial V}{\partial M} - \frac{(1 - e^2)^{1/2}}{na^2 e} \frac{\partial V}{\partial \omega} \quad (4b)$$

$$\frac{d\omega}{dt} = \frac{(1 - e^2)^{1/2}}{na^2 e} \left( \frac{\partial V}{\partial e} \right) \\ - \frac{\cos i}{na^2 (1 - e^2)^{1/2} \sin i} \left( \frac{\partial V}{\partial i} \right) \quad (4c)$$

$$\frac{di}{dt} = \frac{\cos i}{na^2 (1 - e^2)^{1/2} \sin i} \left( \frac{\partial V}{\partial \omega} \right) \\ - \frac{1}{na^2 (1 - e^2)^{1/2} \sin i} \left( \frac{\partial V}{\partial \Omega} \right) \quad (4d)$$

$$\frac{d\Omega}{dt} = \frac{1}{na^2 (1 - e^2)^{1/2} \sin i} \left( \frac{\partial V}{\partial i} \right) \quad (4e)$$

$$\frac{dM}{dt} = n - \frac{1 - e^2}{na^2 e} \left( \frac{\partial V}{\partial e} \right) - \frac{2}{na} \left( \frac{\partial V}{\partial a} \right) \quad (4f)$$

These equations are the result of a direct coordinate transformation of the equations of motion from Cartesian coordinates  $(x, y, z, \dot{x}, \dot{y}, \dot{z})$  to the six classical orbital elements  $(a, e, i, \Omega, \omega, M)$ . Once the nonspherical gravitational contribution of the potential  $V$  is defined, the partial derivatives required for the solution of the Lagrange planetary equations can be evaluated; this evaluation enables the orbit of the spacecraft to be determined. The resulting equations for several of the nonspherical potential terms are contained in appendix A. These first-order analytical equations are derived with an averaging technique that involves integration of the short-period effects in the disturbing function. (See refs. 3 and 11.)

### Mass Concentrations—An Alternative Approach

The spherical harmonic expression for the potential (eq. (3)) is very useful for describing gravitational fields that vary only slightly from a spherical field in a smooth manner, such as for the Earth. A detailed description of the Earth’s potential is obtained with only a few harmonic terms. The Moon is smaller and less massive than the Earth; therefore, it can support more stress per unit mass and has the capability to possess greater gravitational anomalies than does the Earth. Because of its irregular internal structure and surface shape, the Moon has a very complicated gravitational field. As a result of these properties, the Moon’s gravitational field cannot be described with only a few terms.

Several problems are encountered when a spherical harmonic expansion of the potential is used. One problem is the slow convergence of the expansion for points near the lunar surface, where  $\frac{R}{r}$  is slightly less than one. For this reason, many gravitational coefficients are required to describe the orbit of a low-altitude satellite. Also, spherical harmonic expansions are unable to describe localized gravitational anomalies unless a large number of coefficients are introduced; they are more appropriate for describing an average gravitational field. For example, an expansion on the order of 180 ( $m = 180$ , see eq. (3)) is necessary to describe a local anomaly that subtends an angle of  $1^\circ$ . (See ref. 12.) Difficulties in obtaining values of  $C_{nm}$  and  $S_{nm}$  for the Moon have also

been encountered for reasons that are discussed in the section "Lunar Gravity Models."

The existence of lunar mass concentrations (mascons) was postulated in reference 13. These are localized regions of higher than average density that produce measurable gravity anomalies. A gravity anomaly is defined as the residual gravity effect after the attraction of a reference body (such as a homogeneous spheroid, rotational ellipsoid, triaxial ellipsoid, etc.) is subtracted from the measured gravity data (ref. 14). This gravity anomaly is a result of the mascon's higher density (mascons have a density of approximately  $3.3 \text{ g/cm}^3$ , whereas surrounding rocks have an average density of only  $3.0 \text{ g/cm}^3$ ). Mascons constitute between 0.01 and 0.03 percent of the Moon's mass, and their location is coincident with the location of lunar seas (maria). (See ref. 12.) These gravitational anomalies are found primarily along the equator on the near side of the Moon.

Attempts have been made to use mascon models to describe the features of orbital tracking data. Models that distribute mascons below the lunar surface rather than on the surface (ref. 15) and models that treat mascons as circular disks rather than point masses (ref. 16) have had much more success. A model was also developed that treated the mascon as a third body to investigate the short-period, long-period, and secular effects of mascons on the orbit of a spacecraft. (See ref. 17.) The main restriction of this latter approach is that it is not applicable to low-altitude satellites.

One advantage of a spherical harmonic model for lifetime studies is that it can be used to provide a relatively simple analytical approach. Since a spherical harmonic description allows one to average short-period effects (perturbations that result from the variation of the mean anomaly  $M$  around the orbit), these averaging effects can be accounted for over the period of a few orbits. Averaging effects for mascon models can be developed by mapping the mascons to a set of spherical harmonic coefficients. However, this process effectively eliminates the advantage of the mascon approach, because a large number of coefficients are needed to accurately model the effects of mascons.

An alternative method was developed by Ananda to construct a disturbing potential in terms of various parameters of the mascons and the orbital elements. (See ref. 18.) This potential is averaged over an orbit to eliminate the short-period terms. Much of this integration cannot be performed analytically. The averaged potential is determined by numerically evaluating these expressions with Gaussian

quadrature formulas that require considerable computer time. Once the potential is defined, the average rates of the mean orbital elements can be determined by evaluating the derivatives in the Lagrange planetary equations (eqs. (4)). Work is being conducted to develop a method that allows for the application of mascon models without the sacrifice of computer time. (See ref. 19.)

Hybrid models, with both spherical harmonics and mascons, have also been proposed (refs. 16 and 20). Purely mascon models, with a large number of mascons (on the order of 100), require significant computational time. Using a few low-degree spherical harmonic terms to describe global nonspherical contributions decreases the number of mascons required to give a complete description of the lunar gravity field. The function of the mascons in a hybrid model is only to describe localized gravitational effects. This may be the most reasonable gravitational model to use, because it combines the benefits of spherical harmonic models and the mascon approach. However, the application of a hybrid model on the preliminary mission design level may prove to be infeasible because of the excessive computer time demanded by the additional complexity associated with the mascons.

A spherical harmonic model was adopted for the study of orbital lifetimes in this investigation because of the availability of these models. Few mascon models are available, and methods for including the effects of these anomalies in long-term orbital predictions have not been widely developed. Also, since lifetime studies involve averaging effects of the entire gravitational field of the Moon, a spherical harmonic model seems to be more appropriate for this application. Mascon models are more appropriate for situations in which information about localized fields is desired. Some applications might include performing a maneuver with a low-altitude satellite above a gravitational anomaly, or calculation of descent and ascent trajectories to and from a landing site near a mascon. If localized gravitational effects are found that cause significant changes in the orbital elements (either as single events or integrated over time), spherical harmonic representations of the lunar gravity field will need to be abandoned in favor of mascon models.

## Lunar Gravity Models

*Derivation of models.* Spherical harmonic lunar gravity models contain values of the gravitational coefficients  $C_{nm}$  and  $S_{nm}$  that define the nonspherical contributions to the potential field. (See

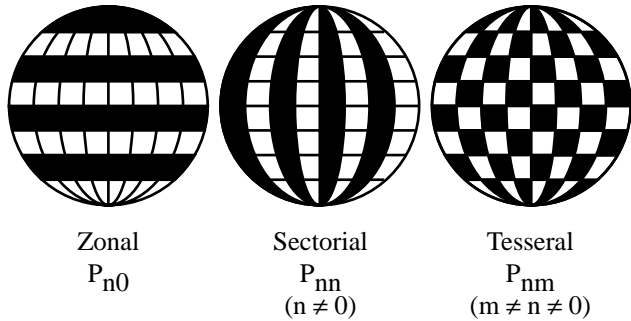


Figure 3. Various types of harmonic coefficients. White area represents elevation above and black area represents elevation below a mean spherical surface. (From ref. 21.)

eq. (3).) There are three types of harmonic coefficients; these types are defined by the values of the subscripts  $n$  and  $m$ . For zonal harmonic coefficients,  $m = 0$  ( $C_{n0}$ , often denoted by  $-J_n$ ). These coefficients describe an axially symmetric potential (in this case, the spin axis of the Moon) independent of the longitude at which the potential is measured. Gravity models for the Earth consisting solely of zonal harmonics yield good approximations to the actual field. However, a longitude dependence in the Moon’s gravity field motivates the need to include other types of coefficients in lunar models. This dependence is introduced by the presence of sectorial and tesseral harmonic coefficients. Sectorial harmonics (where  $n = m \neq 0$ ) give rise to zero values of the potential only along meridians of longitude, whereas tesseral harmonics (where  $n \neq m$ , and  $m$  and  $n$  are nonzero) also give rise to zero values along parallels of latitude. (See fig. 3, from ref. 21.) Once the  $C_{nm}$  and  $S_{nm}$  coefficients are specified, the potential is completely determined as a superposition of the individual harmonic terms.

Further insight into the physical significance of the individual gravitational-coefficient values can be obtained by interpreting the coefficients as surface deviations from a homogeneous sphere. The  $J_2$  gravitational coefficient analytically represents the oblateness of a body (this equatorial “bulge,” common to all rotating bodies, arises from the “centrifugal force” produced by the body’s rotation about its axis). The  $C_{22}$  term describes the ellipsoidal nature (the equatorial ellipticity) of a body, and the  $J_3$  coefficient models the nonspherical mass distribution between the northern and southern hemispheres (the body’s “pear-like” shape). Higher degree gravitational terms describe more localized distributions of mass. Figure 4 (from ref. 22) illustrates the equipotential surfaces for the low-degree zonal harmon-

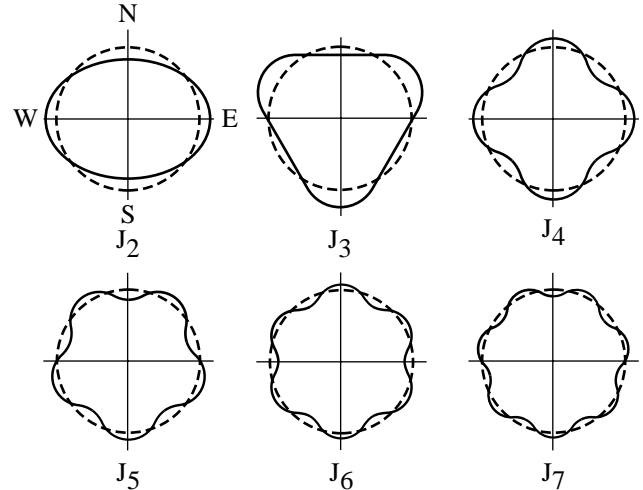


Figure 4. Geometrical shape of Legendre polynomials corresponding to equipotential surfaces for zonal harmonics. The surfaces shown here are for positive values of  $J$  coefficients. (From ref. 22.)

ics. The degree of the term determines the number of lobes of its equipotential surface. As previously mentioned, the zonal equipotential surfaces are independent of longitude and model axially symmetric potentials. The equipotential surfaces associated with the sectorial and tesseral harmonics (figs. 5 and 6) are functions of both latitude and longitude (the  $z$ -axis shown in the figures corresponds to the spin axis of the Moon, and the positive  $x$ -axis is aligned with the Moon-Earth direction). For sectorial and tesseral harmonics, the order of the term represents the number of lobes of a horizontal cross section of its equipotential surface (corresponding to  $\cos m\lambda$  and  $\sin m\lambda$ ).

Values of the gravitational coefficients are determined from radar tracking data of lunar satellites and laser-ranging data measurements. (See ref. 23.) With the Doppler method, the radial velocity of the satellite (the velocity component along the line of sight from the tracking antenna to the spacecraft) is determined from the difference in frequency between the signal emitted by the satellite and the signal received by Earth tracking stations. From these velocity measurements, the radial acceleration can be determined. By attributing this acceleration of the satellite to the gravitational field of the Moon, the potential field (and therefore the value of the harmonic coefficients) can be derived. These coefficients are independent of the orbit of the spacecraft being tracked, because they describe the fluctuations in the gravitational field. However, in practice, the estimated coefficients are dependent on the altitudes

(a) Harmonic coefficient  $C_{22}$ .

(b) Harmonic coefficient  $C_{33}$ .

Figure 5. Geometrical shape of a sectional equipotential surface.

(a) Harmonic coefficient  $C_{31}$ .

(b) Harmonic coefficient  $C_{54}$ .

Figure 6. Geometrical shape of a tesseral equipotential surface.

and inclinations of the satellite data used to derive the model. This dependence is a result of the limited geographic distribution of the measurement set used to compute the coefficients. All effects of the lunar gravity field have not been included in a coefficient model; a set of satellite data covering all regions of the Moon is as yet unavailable. Also, the number of terms included in the gravitational model (the maximum value of the index  $n$ ) also influences the estimated values of the coefficients.

Lunar laser-ranging data are obtained by measuring the round-trip time of a laser pulse between an Earth observatory and a retroreflector array on the surface of the Moon. These measurements allow the Earth-Moon distance to be determined within fractions of a meter, precise enough to monitor the physical librations of the Moon. By observing variations in the lunar rotation, values for the low-degree harmonics can be determined. (See ref. 24.)

**Limitations of existing models.** There are three major obstacles to making an accurate determination of the Moon's gravitational field. (See ref. 25.) First, as previously mentioned, the various surface and interior features make the Moon a very complicated gravitational object, and therefore difficult to model with a simple mathematical representation. Further, gravitational models of high order and degree may not be appropriate for orbital lifetime predictions at the present time, because there is still uncertainty in the values of even some of the lower coefficients, such as  $J_3$ . These uncertainties may overshadow any attempt to adequately model localized variations in the Moon's gravitational field with higher coefficient gravity models.

Second, the range of inclinations and other orbital parameters for which tracking data exist is quite limited. Ample tracking data exist for near-equatorial orbits. However, for midlatitude and near-polar inclinations, little tracking data are available. Since efforts have been made to include only orbital data with trajectories free of propulsive maneuvers (influenced only by the force of gravity), the amount of tracking data available is further limited (ref. 26). High-altitude orbits are ideal for determination of the low-degree harmonic coefficients, because these orbits are not sensitive to the effects of high-degree harmonics. (See ref. 27.) However, most of the lunar satellite tracking data available are for low-altitude orbits. The last U.S. satellites to orbit the Moon were the Explorer probes in the mid-1970's. Little new information about the Moon's gravitational field has been obtained since then.

The inability of Earth-based stations to obtain satellite tracking data as the spacecraft passes behind the Moon is the third obstacle to developing an accurate lunar gravitational model. Because of libration of the Moon's orbit, 41 percent of the lunar surface is never visible from the Earth (ref. 28). As a result of this limitation in tracking data, gravitational effects on the far side of the Moon cannot be practically determined. The absence of a description of the gravitational field on the far side of the Moon remains as the greatest limitation to making accurate predictions of orbital lifetimes for lunar satellites.

**Current models available.** Several lunar gravity models have been constructed, based primarily on satellite tracking data, with the additional use of lunar laser-ranging observations and mass-concentration models. Differences in the values of the gravitational coefficients of these models occur because of the selection of different satellite tracking data and the different methods used to process these data. (See tables 1 and 2.) Coverage from the Apollo satellites is limited to about 20 percent of the lunar surface. (See ref. 29.) Tracking data from Lunar Orbiter 4 and 5 are commonly used to provide high-inclination information, while Apollo 15 and 16 subsatellite tracking data are used to provide low-inclination information.

Six gravitational models were recently compared by the Jet Propulsion Laboratory for the Lunar Observer mission study. (See ref. 30.) The Liu-Laing model (ref. 31), constructed primarily from Doppler data of the five Lunar Orbiter satellites, is an  $8 \times 8$  ( $n \times m$  denotes  $n$ th degree,  $m$ th order, see eq. (3)) model with additional zonal harmonics up to degree 15. This model differs from other models in that the values of the high-degree zonal harmonics are larger than the value of the low-degree zonal harmonics. The Ferrari  $5 \times 5$  model (ref. 23), developed from 9 days of Lunar Orbiter 4 data and approximately 2200 lunar laser-ranging observations, is an attempt to accurately determine the values of the low-degree coefficients. A Ferrari  $16 \times 16$  model (ref. 26) was also developed with Doppler measurements from Lunar Orbiter 5 and Apollo 15 and 16 subsatellites. The Bills-Ferrari  $16 \times 16$  model (ref. 32) used the data sets of the Ferrari  $5 \times 5$  and  $16 \times 16$  models along with a model of approximately 600 mascons. Akim (ref. 33) developed a  $4 \times 4$  model with zonal coefficients  $J_5$ ,  $J_6$ , and  $J_7$ , based on the Soviet Luna spacecraft. A Sagitov  $16 \times 16$  model (ref. 34) also exists, based on data used for the Ferrari  $5 \times 5$  model, the Bills-Ferrari model, and the Akim model, with additional data from Apollo and a mascon model. As mentioned

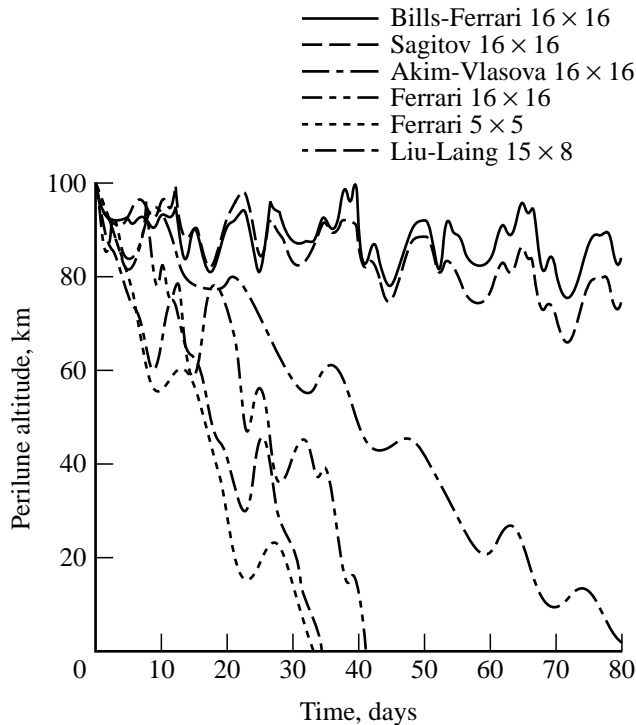


Figure 7. Comparison of six gravitational fields used in JPL Lunar Observer study. Initial 100-km circular polar orbit. (From ref. 35.)

previously, all six of these models are limited by a lack of tracking data for spacecraft on the far side of the Moon and by a scarcity of low-altitude, high-inclination data. Although these models generate similar results for equatorial orbits, the results predicted by these models vary significantly for an initial 100-km-altitude circular polar orbit. (See fig. 7, taken from ref. 35.)

Much debate currently remains as to which gravitational model provides the best predictions of orbital lifetimes for lunar satellites. In the present analysis, the consequences of choosing a particular gravitational model are not emphasized; the focus is centered on the selection of the initial orbital parameters. The Ferrari  $5 \times 5$  model (ref. 23) was chosen for this study for several reasons. First, the computer program used in this analysis (appendix B) is limited to gravity models of degree and order no larger than eight. Second, this model provided a “worst case” scenario for polar orbits, because this gravitational model generated the shortest orbital lifetime predictions in the JPL study. Therefore, this model may overestimate the rate of decay in perilune altitude. However, for mission design purposes, overestimation of the effects due to the Moon’s gravitational field is

more desirable than underestimation. A low-degree model was also desired to avoid addressing the errors and effects of the higher degree harmonics. Although the low-degree model is incapable of modeling localized gravitational anomalies, it provides a global description of the lunar gravity field that is adequate for performing lifetime studies.

## Analysis

The goal in this analysis is to illustrate the impact of the Moon’s gravitational perturbations on the lifetimes of low-altitude, near-circular parking orbits, and to identify orbits favorable for lunar outpost missions (orbits that have the longest orbital lifetimes). A method is provided for mission planners to incorporate nonspherical gravitational effects in preliminary lunar analysis studies.

### Effects of External Forces

The Lagrange planetary equations presented in equations (4a) to (4f) describe the changes in a satellite orbit due to forces that may be expressed in terms of a potential. The equations in appendix A have assumed a potential solely as a result of the lunar gravitational field. To give a complete description of the satellite motion, all forces acting on the satellite must be taken into account. The absence of a significant atmosphere on the Moon eliminates any need to consider drag effects. Forces that could affect the satellite motion include solar radiation pressure and perturbations from other bodies, particularly the Earth and the Sun.

The influence of solar radiation pressure on a low-altitude lunar satellite is examined in this report. (See appendix B.) The resulting acceleration of a satellite is a function of its mass, cross-sectional area, and reflectivity coefficient. A mass of 10.2 metric tons and a cross-sectional area of  $75 \text{ m}^2$  were chosen as values for a lunar excursion vehicle; also, the vehicle was assumed to be a perfect reflector. Solar radiation pressure has the greatest effect on low-inclination orbits, although these effects were small. For a near-circular orbit with an initial altitude of 300 km, solar radiation caused a change in the perilune altitude of less than 1 km over a period of 180 days. Unless a satellite has a large cross-sectional area and small mass, solar radiation effects are negligible.

Although both the Earth and the Sun contribute perturbation effects, the effects due to the Earth are about 170 times larger than the effects due to the Sun. (See ref. 36.) The average effects of a third body

on the eccentricity (the main parameter in orbital lifetime studies) can be expressed as

$$\frac{d\bar{e}}{dt} = \frac{15}{8} \left( \frac{n_3^2}{\bar{n}} \right) \bar{e} (1 - \bar{e}^2)^{1/2} \sin^2 \bar{i} \sin 2\bar{\omega} \quad (5)$$

where the bars denote variables that have been averaged over the period of the third body about the central body and over the period of the satellite. (See ref. 37.) The variable  $n_3$  represents the mean angular motion of the third body about the central body. From equation (5), it is apparent that third-body perturbations have the greatest effect on eccentricity for mid-eccentricity (maximized for  $\bar{e} = 0.707$ ) and high-inclination satellite orbits. The average value of  $\omega$  also strongly influences the effects of the third-body perturbations.

Using the program LUNLIFE with the Ferrari  $5 \times 5$  gravity model, a near-circular, initial 300-km, perilune-altitude polar orbit had a 20-km-higher perilune altitude after 180 days when third-body perturbation effects were included. (See fig. 8.) For an initial 100-km perilune-altitude polar orbit, the orbital lifetime was 157 days when third-body effects were included; the lifetime was only 144 days when Earth-Sun perturbation effects were neglected (fig. 9). Although the effects of third-body perturbations on orbital lifetimes may not be negligible for all orbits, these effects are small for most of the orbits addressed in this investigation (because of the restriction of near-circular parking orbits). Therefore, third-body perturbation effects were not included in this analysis.

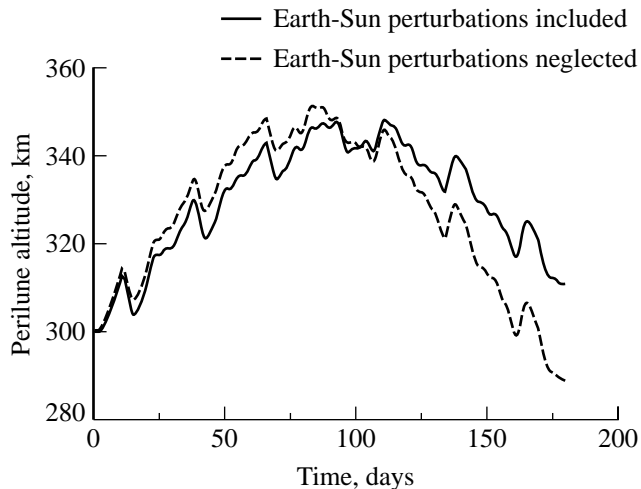


Figure 8. Earth-Sun perturbation effects for 300-km initial perilune altitude polar orbit (using Ferrari model). (Initial conditions:  $i = 90^\circ$ ,  $\Omega = 0^\circ$ ,  $\omega = 225^\circ$ .)

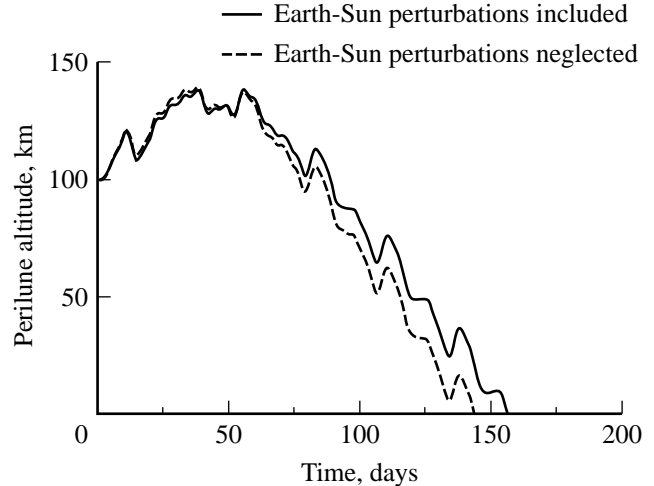


Figure 9. Earth-Sun perturbation effects for 100-km initial perilune altitude polar orbit (using Ferrari model). (Initial conditions:  $i = 90^\circ$ ,  $\Omega = 0^\circ$ ,  $\omega = 225^\circ$ .)

### Use of Orbital Elements for Lifetime Studies

The Lagrange planetary equations of motion (eqs. (4a) to (4f)) are used for orbital lifetime studies, because they enable integration of the classical orbital elements ( $a$ ,  $e$ ,  $i$ ,  $\Omega$ ,  $\omega$ , and  $M$ , see figs. 10 and 11). The mean anomaly  $M$ , defined as the mean angular motion multiplied by the time since pericenter passage, is related to the true anomaly  $\nu$ . The advantage of utilizing orbital elements as opposed to Cartesian coordinates (defining the radius and velocity vectors of the satellite as functions of  $x$ ,  $y$ , and  $z$ ) is that very large integration time steps can be used, because the orbital elements (except for  $M$ ) change very little over consecutive orbits compared with a Cartesian description. Integration over large time steps requires that the short-period effects be averaged for the disturbing function in the Lagrange equations. Time steps of 1 day were used to generate the results in this analysis. To verify that 1-day time steps were not too large to give inaccurate results, test cases were run with the program LUNLIFE with 10-sec time steps. The results generated by these two different step sizes were nearly identical, within 0.01 percent.

The disadvantage of using a classical orbital-element description of the equations of motion involves the inability to directly address certain types of orbits (e.g., circular, equatorial), because some of the elements may not be defined. The classical orbital-element description does not pose a significant restriction in this study, as near-circular ( $e = 0.05$ ) and near-equatorial ( $i = 1^\circ$ , and  $179^\circ$ ) orbits were addressed. (There is a set of orbital

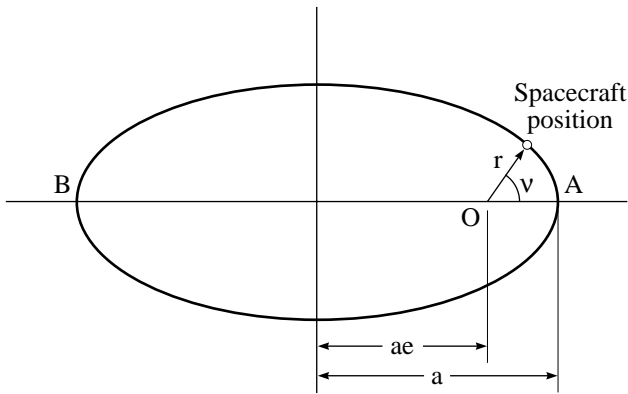


Figure 10. Geometry of an elliptical orbit. (From ref. 21.)

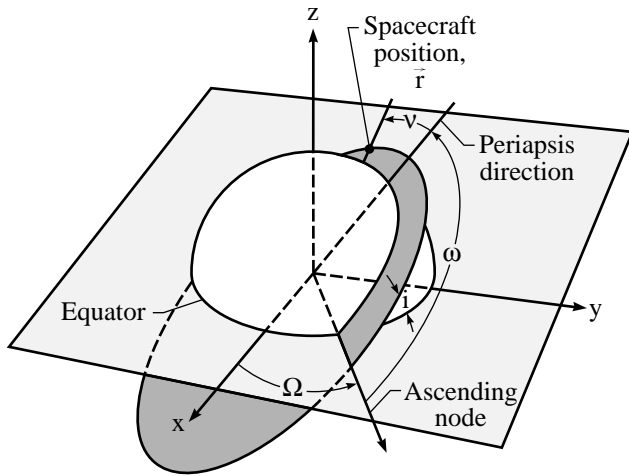


Figure 11. Orbital geometry.

elements, referred to as equinoctial elements, that can address circular and equatorial orbits. (See refs. 30 and 38.) However, equinoctial elements are utilized much less frequently than classical orbital elements.)

Only three of the six orbital elements were monitored in this analysis. Since the mean anomaly  $M$  is used to describe the position of the satellite within the orbit, and not the shape or position of the orbit itself, it need not be considered in determining orbital lifetimes. The semimajor axis experiences only short-period variations, so as it is integrated over the mean anomaly for one period, its average rate of change is zero. Short-period effects in the orbital elements are observed with the program ASAP (Artificial Satellite Analysis Program, ref. 39). The amplitude of short-term variations is small (on the order of 1 km (figs. 12 and 13) and has little effect on orbital lifetime predictions. Hence, the semimajor axis is treated as

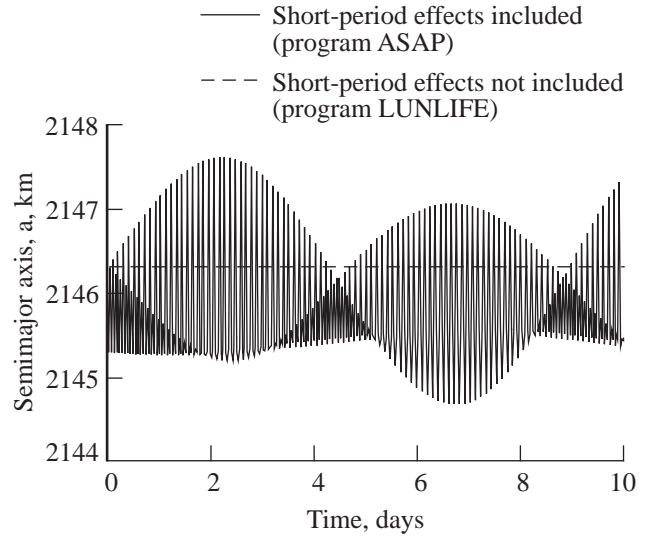


Figure 12. Short-period effects in semimajor axis. (Initial conditions:  $i = 90^\circ$ ,  $\Omega = 0^\circ$ ,  $\omega = 0^\circ$ ,  $h_p = 300$  km; gravity model:  $8 \times 8$  truncation of Bills-Ferrari model.)

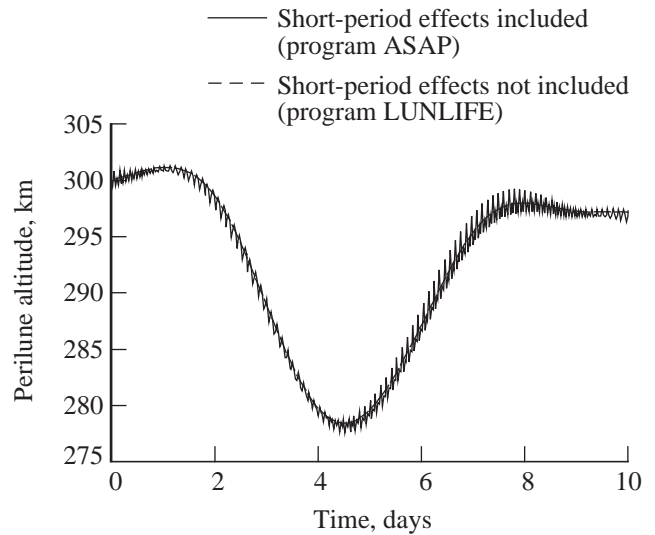


Figure 13. Short-period effects in perilune altitude. (Initial conditions:  $i = 90^\circ$ ,  $\Omega = 0^\circ$ ,  $\omega = 0^\circ$ ,  $h_p = 300$  km; gravity model:  $8 \times 8$  truncation of Bills-Ferrari model.)

a constant in this analysis. Inclination is cyclical and has variations typically on the order of  $1^\circ$  over a 180-day period. (See fig. 14.) As with the semimajor axis, the inclination can be treated as a constant with little loss of accuracy (although changes in inclination were included in this analysis). The remaining orbital elements that change significantly over the time periods studied in this analysis (other than the mean anomaly) are eccentricity, longitude of ascending node, and argument of perilune.

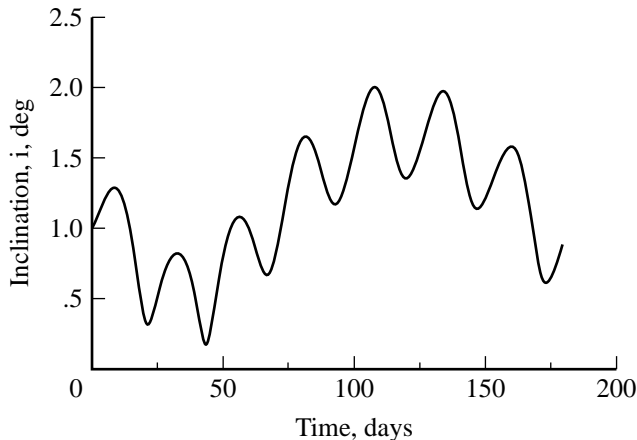


Figure 14. Typical inclination versus time plot. (Initial conditions:  $i = 1^\circ$ ,  $\Omega = 0^\circ$ ,  $\omega = 0^\circ$ ,  $h_p = 100$  km.)

The key parameter in orbital lifetime studies is the perilune altitude (or equivalently, the eccentricity, since the perilune altitude is a function of the eccentricity). The life of the satellite orbit is terminated when the magnitude of the perilune radius of the satellite falls below the value of the average radius of the Moon; the satellite then impacts the surface. The perilune radius is given as:

$$r_p = a(1 - e) \quad (6)$$

Simple differentiation, assuming the semimajor axis  $a$  remains constant, yields

$$\Delta r_p = -a \Delta e \quad (7)$$

The rate of change in perilune altitude is directly proportional to the rate of change in eccentricity. Near-zero or negative rates of change (orbit becomes more circular) in eccentricity enable orbital lifetimes to be maximized. Since the rate of change in eccentricity is a function of initial inclination, longitude of ascending node, and argument of perilune (eqs. (A2b), (A3b), and (A5b)), these initial orbital parameters directly affect the orbital lifetime. Perilune altitude is also indirectly affected by the rates of change in longitude of ascending node and argument of perilune.

The initial orbital parameters were chosen to include many types of parking orbits that would be of interest to mission planners. The initial eccentricity was fixed at 0.05, small enough for the orbit to be considered nearly circular, yet large enough to avoid any singularities in the computer program associated with circular (zero-eccentricity) orbits. Circular parking orbits are attractive to mission planners,

because they simplify phasing requirements for descent to and ascent from the lunar surface, and simplify phasing requirements for an Earth-return burn (although higher  $\Delta V$  values are required to achieve circular parking orbits). Circular parking orbits are also generally preferred for mapping missions of the Moon's surface. For this study, initial perilune altitudes of 100 km and 300 km, referenced to the mean value of the radius of the Moon, were selected. The specific inclination value of a parking orbit selected for a particular mission will be heavily influenced by the desired mission objectives and the location of lunar landing sites. In this analysis, both direct and retrograde orbits are addressed. Lifetime results were first generated by varying initial values of longitude of ascending node and argument of perilune over  $360^\circ$  for a specific initial value of inclination. Since orbital lifetimes were weakly influenced by initial values of longitude of ascending node (small effect of the sectorial and tesseral harmonics on lifetimes), lifetime results were generated by varying initial values of inclination and argument of perilune for fixed values of initial longitude of ascending node.

## Results and Discussion

### Development of a Simplified Gravitational Model

The need to analyze orbital lifetimes for a large number of initial orbital parameters motivated the formulation of a simplified gravitational field model. Although the program LUNLIFE was capable of generating the lifetime of a given orbit relatively quickly with the Ferrari  $5 \times 5$  gravitational model, excessive computer time (on the order of 100 hours) would have been required to generate the large number of results desired in this analysis. For example, to generate contour plots of lifetimes versus initial argument of perilune and initial longitude of ascending node to a resolution of a  $5^\circ$  by  $5^\circ$  grid, the evaluation of approximately 5000 orbital lifetimes was necessary. By neglecting many of the coefficients in the Ferrari  $5 \times 5$  model and using a simplified integration technique (a single-step integration of the first-order equations of the orbital rates instead of a multiple-step numerical integration of the complete equations as given in ref. 40), a more efficient method was devised to predict orbital lifetimes. This method reduced the required computation time by approximately two orders of magnitude without appreciably sacrificing accuracy (less than 5 percent) in the prediction of orbital lifetimes.

Previous studies have attempted to approximate the Moon's gravitational field by using only a few

harmonic coefficients. A four-coefficient lunar gravity model was developed in the 1960's (based on Lunar Orbiter tracking data) for Apollo mission control. (See ref. 3.) The formulation of this simplified model was necessitated by the restrictions of onboard computing capabilities at that time. The coefficients  $J_2$ ,  $J_3$ ,  $C_{22}$ , and  $C_{31}$  were selected for this model because it was determined that they had the greatest effect on the orbital elements. The model was limited in its design to accommodate only initial orbital elements similar to the Lunar Orbiter missions. A similar simplified model that was developed for this analysis has been validated for the entire range of values of initial inclination, argument of perilune, and longitude of ascending node.

A reduction in the number of computations also allowed for the possibility of implementing optimization routines to maximize orbital lifetimes. An attempt was initially made to utilize optimization methods for selecting the initial orbital elements that yielded maximum lifetimes. However, this approach was deemed infeasible because of the highly non-linear nature of the problem. The optimization results were also dependent on the initial guess, because the orbital lifetimes objective function was characterized by many local maximum and minimum values.

Several issues were taken into account when selecting the coefficients for the simplified lunar gravitational model. First, an effort was made to retain all the terms used in the Apollo mission control model. Second, the numerical values of the coefficients were examined to decide which ones could be eliminated. (See table 1.) An attempt was made to keep as many zonal terms as possible, because they are responsible for secular effects and are therefore significant in orbital lifetime studies (the  $J_4$  term was eventually discarded because of its small magnitude). Finally, the lower order coefficients were assumed (and later verified) to have a greater effect on the variation in the orbital elements than the higher order terms. A sample case was selected and analyzed with the full Ferrari  $5 \times 5$  model. Individual coefficients were discarded, and the sample case was evaluated and compared with the full model after each term was eliminated. All the  $S_{nm}$  terms were quickly eliminated because of their small value. The higher order  $C_{nm}$  terms were eliminated for the same reason. The final coefficients selected for the simplified model consisted of the same terms as the Apollo mission control model ( $J_2$ ,  $J_3$ ,  $C_{22}$ , and  $C_{31}$ ), with the addition of the  $J_5$  term. The values of these coefficients were adopted directly from the Ferrari  $5 \times 5$  model. An attempt to eliminate the  $J_5$  term drastically changed

the lifetime results. This change indicated the need to include the  $J_5$  term when performing orbital lifetime predictions for long lunar stay times with the Ferrari  $5 \times 5$  model.

The orbital lifetime results generated with the simplified five-coefficient model corresponded closely to the results generated with the Ferrari  $5 \times 5$  model (appendix C). Comparisons of the plots of the orbital elements versus time for the two models illustrate the higher resolution prediction capability of Ferrari's model. (See figs. 15 and 16.) The simplified model contains fewer coefficients to contribute periodic effects and thus simplifies the shapes of the graphs.

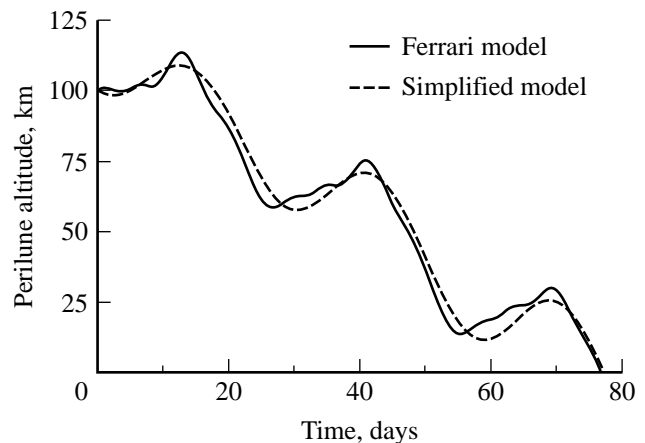


Figure 15. Comparison of perilune altitude for simplified and Ferrari models. (Initial conditions:  $i = 120^\circ$ ,  $\Omega = 0^\circ$ ,  $\omega = 225^\circ$ ,  $h_p = 100$  km.)

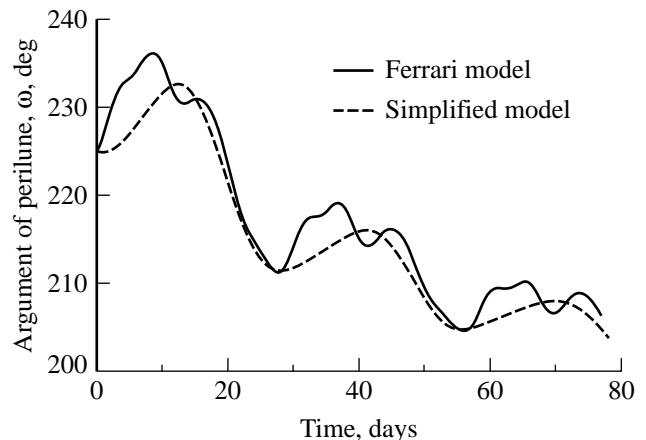


Figure 16. Comparison of argument of perilune altitude for simplified and Ferrari models. (Initial conditions:  $i = 120^\circ$ ,  $\Omega = 0^\circ$ ,  $\omega = 225^\circ$ ,  $h_p = 100$  km.)

The simplified five-coefficient gravity model was an important tool for generating results quickly and for simplifying the interpretation of the final results.

Since first-order analytical equations for the orbital rates are readily available in the literature (eqs. (A1) to (A5)), a simple single-step integration scheme can be used with these equations. For example, the integration of eccentricity is performed by using the equation

$$e_{\text{new}} \approx e_{\text{old}} + \left(\frac{de}{dt}\right) \Delta t \quad (8)$$

where  $\Delta t$  represents the finite-integration time step and  $\frac{de}{dt}$  represents the superposition of the eccentricity rates of change contributed by each gravitational coefficient (assumed to be constant over the time step  $\Delta t$ ). Generating the major effects of the Ferrari  $5 \times 5$  model with only a few coefficients also aided in the interpretation of the results. Since first-order equations existed for each coefficient in the simplified model, analytical methods could be applied to explain the effects of individual coefficients and the superposition of these effects.

### Effects of Individual Gravitational Coefficients

The gravitational coefficients in the simplified gravitational model give rise to both secular and periodic effects. To first-order analysis, secular effects are produced only by the zonal harmonic terms. Both the zonal ( $J_2$ ,  $J_3$ , and  $J_5$ ) and the off-diagonal terms ( $C_{22}$ ,  $C_{31}$ ) in this model are responsible for periodic effects. Coefficients in the lunar gravitational model give rise to short-period, medium-period, and long-period variations. The short-period effects (on the order of the satellite's orbital period) were not modeled in this analysis. These effects can be neglected to first approximation, because the rates of change of these effects often average to zero, as is the case for the semimajor axis. The medium-period terms, commonly referred to as the lunar  $m$ -daily terms, are on the order of a lunar day, or 27.3 Earth days. The influence of this period can be easily seen in the plots of the orbital elements versus time (figs. 17 and 18). A sectorial or tesseral harmonic term of order  $m$  produces medium-period effects with a period of about  $27.3/m$  days (the exact period varies slightly as a result of precession of the longitude of ascending node). Higher order harmonic terms have less influence on long-term orbital lifetime studies, because short-period effects are integrated out more quickly than long-period effects. Long-period effects, on the order of a year, can also be observed in the variations of some of the orbital elements. These effects, contributed by the zonal harmonics, arise from the secular variation of  $\omega$ . The long-period effects are important for lifetime studies, because they produce the largest contribution in perilune-altitude de-

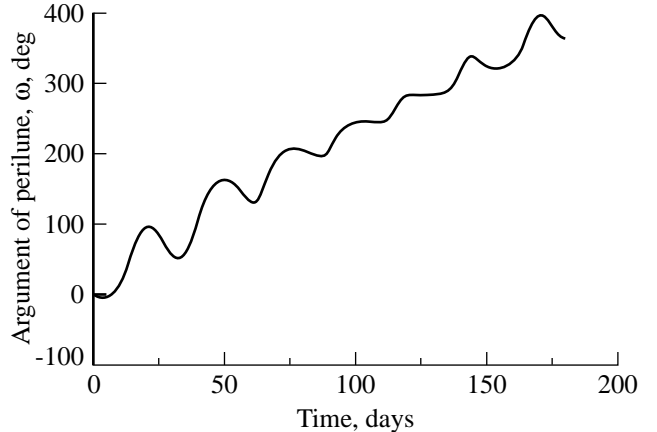


Figure 17. Medium-period effects in argument of perilune for Ferrari model. (Initial conditions:  $i = 179^\circ$ ,  $\Omega = 0^\circ$ ,  $\omega = 0^\circ$ ,  $h_p = 100$  km.)

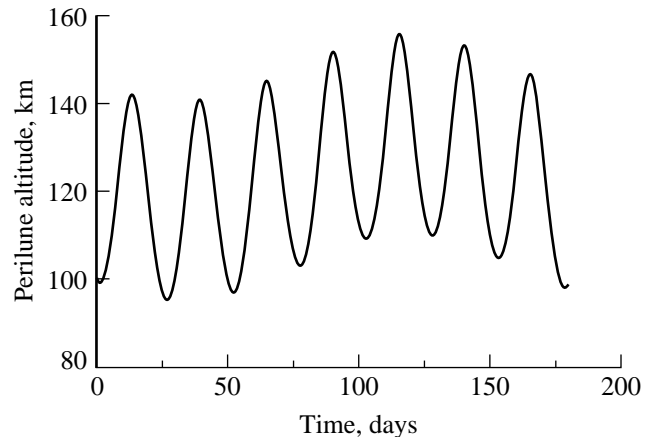


Figure 18. Medium-period effects in perilune for Ferrari model. (Initial conditions:  $i = 179^\circ$ ,  $\Omega = 0^\circ$ ,  $\omega = 0^\circ$ ,  $h_p = 100$  km.)

crease rates over long periods of time and behave as secular effects for orbits with lifetimes of less than a year.

The rates of change in  $e$ ,  $\Omega$ , and  $\omega$  are directly proportional to the values of the gravitational coefficients, although not every coefficient causes a change in every orbital element. (See table 3.) The  $J_2$  term is the dominant term for determining the rate of change of longitude of ascending node. This term and the  $C_{31}$  term also influence the rate of change in argument of perilune. The  $J_3$ ,  $J_5$ , and  $C_{31}$  terms directly affect the rate of change in eccentricity and, therefore, perilune altitude. The final term in the simplified model,  $C_{22}$ , primarily influences the orbital inclination.

## Orbital Lifetime Study

A single-step (Euler) integration technique was used with the simplified five-coefficient gravity model to generate all results in this analysis. Once initial orbital elements were specified, a particular orbit was analyzed for a period of 365 days, unless the lifetime of the orbit expired in less than a year (in which case the analysis was halted immediately). If the lifetime was less than 365 days, the actual value of the lifetime is presented. If the lifetime exceeded 365 days, the minimum perilune altitude attained during the 365-day period is presented. The program LUNLIFE, which uses the complete Ferrari  $5 \times 5$  gravity model, was periodically employed to provide validation for lifetime predictions of individual orbits.

The terms  $J_3$ ,  $J_5$ , and  $C_{31}$  were the only coefficients considered that directly affect rates of eccentricity and, therefore, orbital lifetimes. Unlike the zonal harmonic coefficients, the eccentricity rate for  $C_{31}$  is a function of initial longitude of ascending node and introduces medium-period effects with a period of about 27.3 days. This term has a dramatic effect on rates of eccentricity (but these are only localized effects), and gives rise to step-function behavior in plots of lifetime (fig. 19). This figure directly illustrates the effect that  $C_{31}$  has on orbital lifetimes.

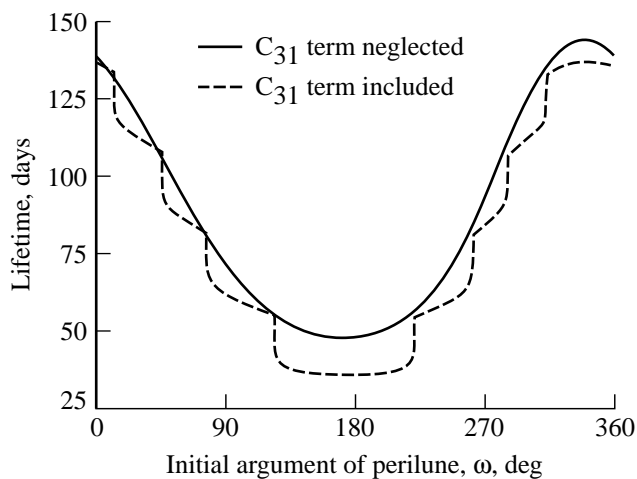
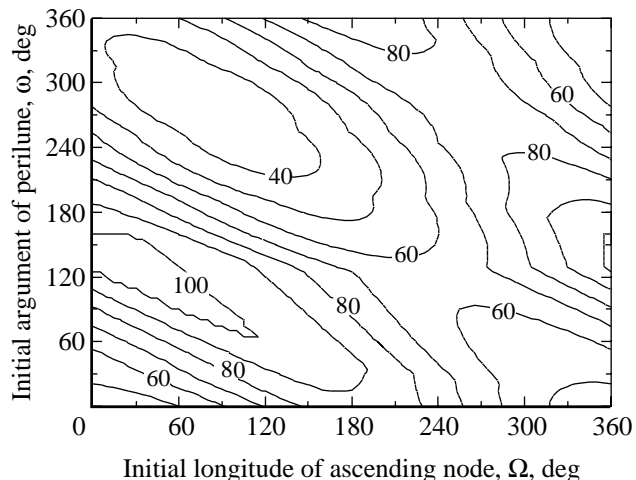
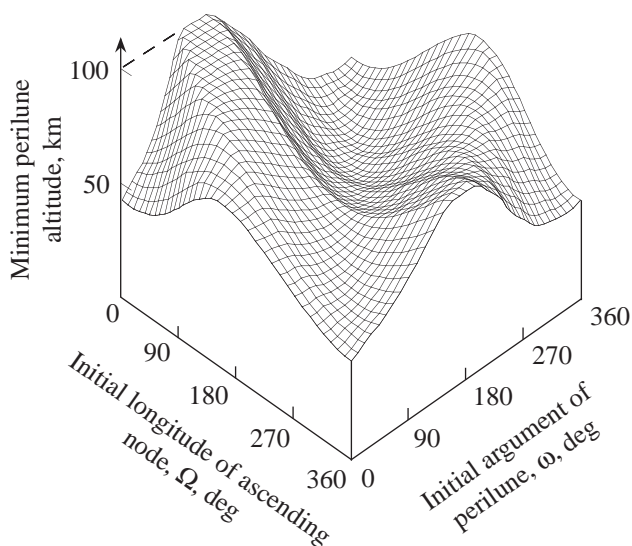


Figure 19. Step-function behavior in lifetimes profile due to  $C_{31}$  term ( $i = 55^\circ$ ).

The step-function shape of the lifetime plot is a result of the superposition in eccentricity rates between  $C_{31}$  and the zonal coefficients. The  $C_{31}$  term contributes large medium-period effects, but the  $J_3$  and  $J_5$  terms contribute long-period effects. When the  $C_{31}$  decay rate is of the same sign as the zonal decay rate, the result is a sharp drop or rise in orbital



(a) Contour plot.



(b) Three-dimensional plot.

Figure 20. Minimum perilune altitude dependence on initial  $\Omega$  and  $\omega$  for low inclinations ( $i = 3^\circ$ ). 100-km initial perilune altitude over a 365-day period.

lifetimes. When the  $C_{31}$  decay rate is of the opposite sign of the zonal decay rate, the total decay rate is nearly zero; this low rate results in plateaus in the plot of orbital lifetimes.

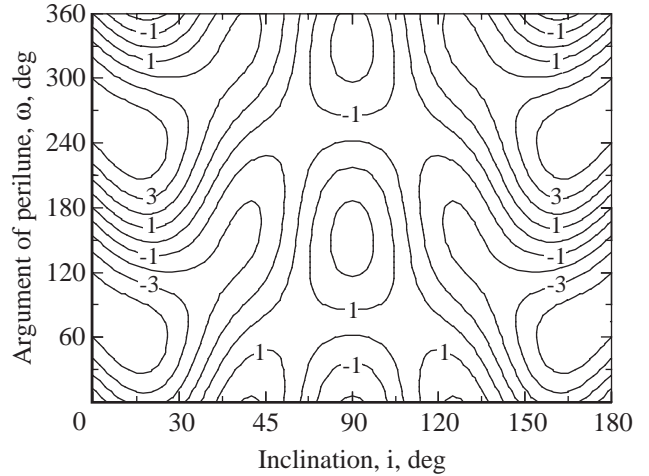
The effect of initial longitude of ascending node on orbital decay rates was significant. Although orbital lifetime results appear to be dependent on the initial longitude of ascending node for near-equatorial orbits (less than  $10^\circ$  inclination), they are actually dependent on the sum of longitude of ascending node and argument of perilune. Figure 20

shows the variation in minimum perilune altitude as a function of initial argument of perilune and longitude of ascending node for a 100-km initial perilune-altitude orbit with a  $3^\circ$  inclination. As shown in this figure, various initial orbital conditions are not described by independent values of  $\Omega$  and  $\omega$ , but rather by values of  $\Omega + \omega$ . For this reason, orbital lifetimes are nearly the same for orbits along lines of constant  $\Omega + \omega$ . (See fig. 20(a).) Lifetime results were subsequently generated by varying the initial argument of perilune and inclination over the entire range of possible values. These results are independent of the initial longitude of ascending node, although slight differences in the results will arise, depending on the value of  $\Omega$ .

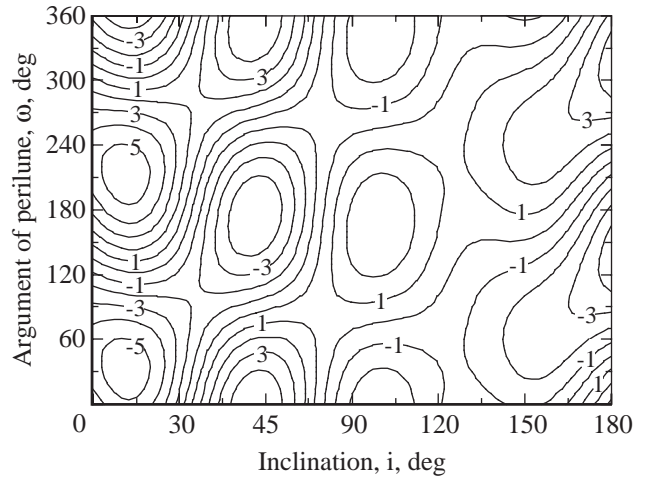
Figures 21(a) to 21(c) show the instantaneous perilune altitude decay rates for  $\Omega = 0^\circ$ ,  $45^\circ$ , and  $90^\circ$ . Although these plots exhibit different characteristics for different values of  $\Omega$ , similar orbital lifetime results will occur regardless of the value of  $\Omega$ , because the effects due to  $\Omega$  will average out to zero after a period of 27.3 days. The plots only illustrate the instantaneous decay rates. To generate valid orbital lifetime predictions, these decay rates must be integrated over time. Although the inclination varies little, the value of argument of perilune may change greatly. An orbit with a given set of initial conditions such that the altitude decay rate is large may evolve over time to a set of conditions for which the decay rate is extremely small (primarily caused by a variation in argument of perilune); therefore, integrated lifetimes longer than those inferred from the figures may be exhibited. Nevertheless, the figures of perilune altitude decay rates are useful in illustrating the magnitude of decay that a lunar satellite can experience in a day.

An integration of the orbital element rates for orbits of various initial conditions was utilized to produce figure 22. The large white regions occur where the initial orbital parameters had a lifetime in excess of 365 days. The results display a symmetry about  $i = 90^\circ$ , which is violated slightly by the presence of a cosine  $i$  term in some of the orbital element rate equations. The closely spaced contour lines in the figure are the result of localized effects due to the  $C_{31}$  coefficient.

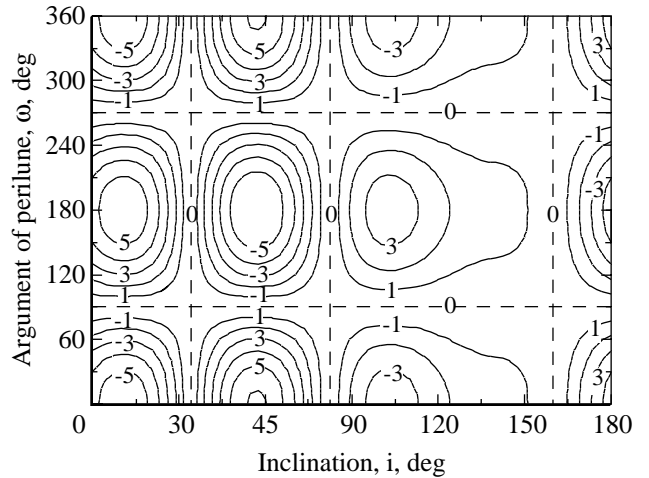
Five bands of short-lifetime orbits occur for specific values of inclination. The appearance of these bands can be explained by examining the perilune altitude decay rates (directly proportional to the negative of the eccentricity rates, see eq. (7)) for  $J_3$  and  $J_5$  as a function of inclination. (See fig. 23.) Figure 23



(a)  $\Omega = 0^\circ$ .



(b)  $\Omega = 45^\circ$ .



(c)  $\Omega = 90^\circ$ .

Figure 21. Perilune-altitude decay rates in km/day versus  $i$  and  $\omega$ .

Figure 22. Contour plot of orbital lifetimes in days for initial longitude of ascending node of  $0^\circ$ . Large white regions represent lifetimes longer than 1 year.

Figure 23. Dependence of rate of change in perilune altitude on inclination for  $J_3$  and  $J_5$  terms. 100-km initial perilune altitude.

was generated by multiplying equations (A3b) and (A2b) by  $-a$  and plotting them, with the initial orbital conditions and  $\omega = 0$ . (All terms proportional to  $e^2$  in the  $\frac{de}{dt}$  equation for  $J_5$  were neglected, because their contribution is small for near-circular orbits.) The difference in the amplitudes of the waveforms illustrates that contributions to the decay rate are much larger for  $J_5$  than for  $J_3$  in the Ferrari model. The bands of short-lifetime plots roughly correspond to the minimum and maximum peaks of the  $J_5$  eccentricity rate ( $i = 19.42^\circ, 56.14^\circ, 90^\circ, 123.86^\circ, \text{ and } 160.58^\circ$ ) and are slightly offset as a re-

sult of contributions from the  $J_3$  term. Also, bands of long-lifetime orbits correspond to zero values of the eccentricity rates for the  $J_5$  coefficient ( $i = 0^\circ, 40.09^\circ, 73.43^\circ, 106.57^\circ, 139.91^\circ, \text{ and } 180^\circ$ ).

The  $J_5$  coefficient is the main driver in the Ferrari model for predicting lifetime effects. Further evidence of the  $J_5$ -term dominance is shown in figure 24. This plot of orbital lifetimes as a function of initial argument of perilune and initial inclination was generated with the  $J_3$  and  $C_{31}$  coefficients set equal to zero. This figure is similar to figure 22, which included effects from  $J_3$  and  $C_{31}$ , and shows that the  $J_5$  term contributes the dominant effect to perilune altitude decay, although the effects from  $J_3$  and  $C_{31}$  are certainly not negligible. (See figs. 19 and 23.)

Figure 24. Contour plot of lifetimes in days for initial longitude of ascending node of  $0^\circ$ . 100-km initial perilune altitude; effects of  $J_3$  and  $C_{31}$  are neglected.

Results were also generated for initial perilune altitudes of 300 km. Figure 25 is a plot of minimum perilune altitude as a function of initial argument of perilune and inclination. The regions at inclination values of approximately  $55^\circ, 90^\circ, \text{ and } 125^\circ$  represent areas where the orbit crashes in less than a year. Although the orbital decay for the higher altitude orbit is less than for the 100-km case, the pattern for the 300-km case is very similar. This analysis focuses primarily on the 100-km initial altitude case, with the assumption that results for this case can be correlated with the 300-km initial altitude case.

### Sensitivity Studies—An Assessment of Uncertainty in Gravitational Field

As previously mentioned, many problems have been encountered in developing an accurate description of the Moon's gravitational field. Figure 7 illustrates the discrepancies among the current available

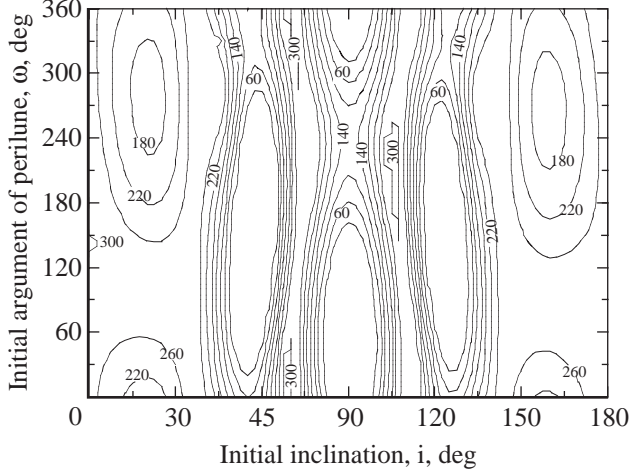


Figure 25. Contour plot of minimum perilune altitude in km over a 365-day period. 300-km initial perilune altitude.

models. Two questions naturally arise: How accurately are the coefficients in the Ferrari  $5 \times 5$  model known (how much error is associated with each coefficient?) and is the Ferrari model (or any other model) an accurate description of the actual lunar gravitational field? The second question is beyond the scope of this investigation, but the first question can be addressed by examining the standard deviations in the values of the gravitational coefficients stated for the Ferrari  $5 \times 5$  model. More importantly, the possible error in orbital lifetime predictions as a result of the uncertainty in the gravitational coefficients can be addressed with the use of sensitivity coefficients.

The formulation of the simplified gravitational model illustrated that five coefficients were adequate to explain the effects due to the Ferrari model on an orbiting lunar satellite. Hence, a good estimate of the errors associated with the uncertainty in the value of the coefficients for the Ferrari model can be obtained by considering only the uncertainties of the five coefficients included in the simplified model; these five coefficients have the greatest influence on the orbital element rates. Furthermore, since only three of these coefficients ( $J_3$ ,  $J_5$ , and  $C_{31}$ ) directly affect the eccentricity rates (the  $J_2$  and  $C_{22}$  terms indirectly affect the eccentricity rates by causing changes in the other orbital elements), the error in orbital lifetime predictions associated with the uncertainty of the coefficients in the Ferrari model can be approximated by addressing the uncertainty solely in these three harmonic terms.

The sensitivity coefficients for each gravity coefficient are shown in figures 26 to 28. The sensitivity

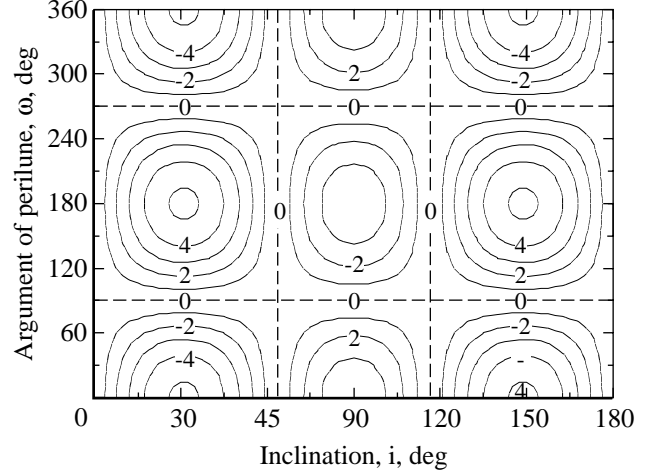


Figure 26. Contour plot of sensitivity for  $J_3$  in units of  $\text{km/day} \times 10^4$  ( $\Omega = 0^\circ$ ) for  $h_p = 100$  km.

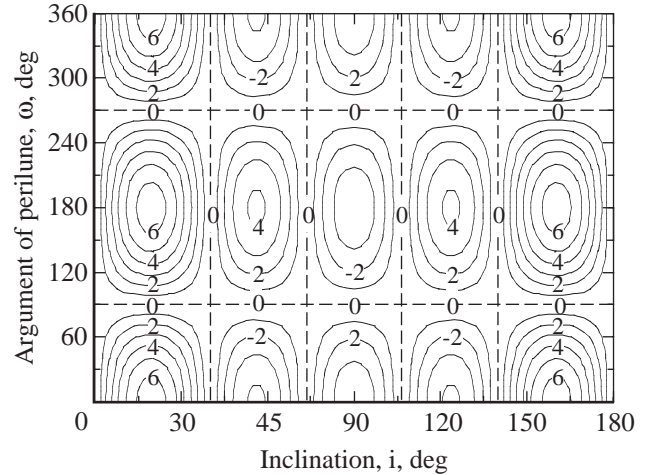


Figure 27. Contour plot of sensitivity for  $J_5$  in units of  $\text{km/day} \times 10^4$  ( $\Omega = 0^\circ$ ) for  $h_p = 100$  km.

coefficients were obtained by differentiating the rate of change in perilune altitude (the first-order analytical equation associated with each coefficient, see eqs. (7), (A2b), (A3b), and (A5b)) with respect to the given gravitational coefficient. Since the rates of change in perilune altitude vary linearly with the gravitational coefficients, the sensitivity coefficients are independent of the values of the coefficients in a gravitational model. As a result, figures 26 to 28 can be interpreted in two ways: These figures represent a “normalized” rate of change in perilune altitude, independent of the value of the gravitational coefficients, or they serve as a means of illustrating the sensitivity of the perilune altitude decay rate with respect to the uncertainty in the value of the particular coefficient. The contours of these figures are in

units of  $\text{km/day} \times 10^4$ . Plots of the sensitivity coefficients for a 300-km initial perilune altitude orbit exhibited the same pattern as for the 100-km case, although the values of the sensitivity coefficients were roughly only half as large.

To evaluate the error in orbital lifetime predictions associated with the Ferrari model, the variance in the perilune decay rate was calculated with the following formula:

$$\sigma_{\dot{r}_p} = \left[ \left( \frac{\partial \dot{r}_p}{\partial J_3} \sigma_{J_3} \right)^2 + \left( \frac{\partial \dot{r}_p}{\partial J_5} \sigma_{J_5} \right)^2 + \left( \frac{\partial \dot{r}_p}{\partial C_{31}} \sigma_{C_{31}} \right)^2 \right]^{1/2} \quad (9)$$

(a)  $\Omega = 0^\circ$ .

(b)  $\Omega = 45^\circ$ .

(c)  $\Omega = 90^\circ$ .

where  $\dot{r}_p$  is the perilune altitude rate of change for the corresponding coefficient (the gravitational coefficients in the numerator of equation (9) appear as subscripts of  $\dot{r}_p$ , not as values of the coefficients themselves) and  $\sigma$  is the corresponding standard deviation of each gravitational coefficient value. In using this formula, no correlation in the uncertainties of the values of the gravitational coefficients is assumed. However, the  $J_3$  and  $J_5$  coefficients are highly correlated. Since these coefficients affect the orbital elements in a similar manner (table 3), separating the effects that are individually contributed by these coefficients is difficult. By not accounting for correlation effects, equation (9) overestimates the errors associated with the uncertainties in the values of  $J_3$ ,  $J_5$ , and  $C_{31}$  (if the  $J_3$  and  $J_5$  terms are dominant, the errors may be significantly overestimated).

For the Ferrari model (ref. 23),  $\sigma_{J_3} = 1.8 \times 10^{-6}$ ,  $\sigma_{J_5} = 2.0 \times 10^{-5}$ ,  $\sigma_{C_{31}} = 1.9 \times 10^{-6}$ . Figures 29(a) to 29(c) show the variance in perilune decay rate in units of  $\text{km/day}$  for  $\Omega = 0^\circ$ ,  $45^\circ$ , and  $90^\circ$ . The similarity in these plots indicates that the uncertainty in the value of the  $C_{31}$  coefficient contributes little to the overall error in orbital lifetime predictions. The similarity between the variance plots and the sensitivity coefficient plot for  $J_5$  (fig. 27) indicates that the error in orbital decay rates for the Ferrari model is due almost entirely to the uncertainty in the value of the  $J_5$  coefficient. In fact, the standard deviation associated with  $J_5$  is an order of magnitude larger than the standard deviations for  $J_3$  and  $C_{31}$ .

As with the figures of the perilune altitude decay rates (fig. 21), the variance plots convey only instantaneous information. To assess the uncertainty in the perilune altitude at the end of an orbit's lifetime,

Figure 28. Contour plot of sensitivity for  $C_{31}$  in units of  $\text{km/day} \times 10^4$  for  $h_p = 100$  km.

(a)  $\Omega = 0^\circ$ .

(a) Integrated variance in kilometers.

(b)  $\Omega = 45^\circ$ .

(b) Lifetime in days.

Figure 30. Orbital lifetime characteristics for 100-km initial perilune altitude and  $\Omega = 0^\circ$ .

the variance must be integrated over time. The computer program was modified to integrate the variance in a manner similar to the integration of the orbital elements (eq. (8)); this integration resulted in figure 30(a). To interpret the figure, one must also refer to the plot of orbital lifetimes (fig. 30(b)). For example, a parking orbit with  $i = 40^\circ$  and  $\omega = 120^\circ$  has a lifetime of more than 360 days (fig. 30(b)). However, this orbit has an uncertainty of approximately  $\pm 40$  km in the final perilune altitude as a result of the inaccuracy in the gravitational coefficients (fig. 30(a)).

The uncertainty in perilune altitude is less for orbits with short lifetimes, because the errors in the decay rates have less time to accumulate. The largest uncertainties in perilune altitude occur for

(c)  $\Omega = 90^\circ$ .

Figure 29. Contour plot of  $\dot{r}_p$  variance in km/day versus  $i$  and  $\omega$  for an initial  $h_p = 100$  km.

orbits with lifetimes longer than a year. The uncertainties in the final values of perilune altitude range from 20 km to 300 km; this range demonstrates the inadequacy of current models for making long-term predictions of the orbital elements. A decrease in the uncertainty in perilune altitude values by an order of magnitude (which can only be achieved by decreasing the uncertainty in the values of the gravitational coefficients themselves) is required to provide mission planners with acceptable orbital lifetime predictions over the time periods addressed in this analysis.

### Applications of Analysis

Although the uncertainty of the coefficients in the Ferrari model creates difficulty in generating long-term orbital predictions, this analysis illustrates a technique to address effects of the nonspherical mass distribution of the Moon on a low-altitude near-circular orbit. The usefulness of introducing a simplified gravitational model when performing orbital lifetime studies at the preliminary mission design level has also been demonstrated. The Ferrari gravitational model was specifically chosen for the purpose of illustrating techniques for determining orbital lifetimes to enable quantitative results to be generated. However, several criteria can be applied from this analysis to assess the qualitative effects of other models on orbital lifetimes. These criteria indicate the important parameters involved in lifetime predictions.

Investigation of the  $C_{31}$  gravitational coefficient illustrates that off-diagonal terms may have a significant effect on perilune altitude decay rates. However, these effects are periodic, with a 27.3-day cycle, and have little influence on long-term lifetime predictions. Therefore, the consequences of lunar gravity fields on long-term orbital predictions are dependent mainly on the odd zonal harmonics, because they have the greatest effect on the eccentricity rates. The odd zonal coefficients model the geometrical asymmetry between the northern and southern hemispheres. Although both hemispheres contain the same amount of mass, the distribution of the mass within the two hemispheres is not the same. (See ref. 22.) This mass distribution results in a long-period variation in the eccentricity. These variations are proportional to  $(R/a)^n$ , where  $n$  is the degree of the zonal term. (See ref. 4.) For high-altitude orbits, the effects due to higher order terms are attenuated. However, for low-altitude orbits (such as the ones considered in this analysis),  $R/a$  converges slowly and enables higher order terms to contribute significantly. The figures of the sensitivity coefficients

(figs. 26 to 28) can be used to calculate the rate of decay of perilune altitude for any specified value of the gravitational coefficients. Although the rates must be integrated to determine orbital lifetimes, a comparison of the rates indicates which terms in the gravitational model provide significant contributions to altitude decay and shows the effect of decay rates as a function of inclination.

For the Ferrari model, the  $J_5$  coefficient contributed the primary influence in orbital lifetimes (and the primary source of error); this influence indicates that long lifetimes exist near inclinations of  $40.09^\circ$  and  $73.43^\circ$ , where the eccentricity rates for  $J_5$  are zero for near-circular orbits (eq. (A3b)). For other gravitational models, more than one gravitational coefficient may strongly influence orbital lifetimes. The eccentricity rate for  $J_3$  is zero for an inclination of  $63.43^\circ$ . These results indicate that if  $J_3$  and  $J_5$  are the dominant odd zonal terms of the gravitational field and are of the same sign, long-lifetime orbits will exist somewhere within a  $10^\circ$  inclination band (between  $63.43^\circ$  and  $73.43^\circ$ , figs. 22 and 23). However, if the sign of  $J_5$  is negative (the actual sign of  $J_5$  is still unknown), a long-lifetime band of orbits will exist somewhere between inclination values of  $40.09^\circ$  and  $63.43^\circ$ . These types of low-altitude, near-circular orbits are ideal for mission planners that want low rates of decay in perilune altitude (corresponding to a low  $\Delta V$  budget for altitude boost maneuvers) and high inclination. (High inclination orbits are ideal for obtaining maximum coverage for a mapping mission or for providing rendezvous capability over a large range of landing-site latitudes for a manned mission.)

A general observation can also be made about the lifetimes of polar orbits that are predicted by various spherical harmonic models. As a function of inclination, the  $\frac{de}{dt}$  value that corresponds to each odd zonal harmonic will have a local minimum or maximum (dependent on the sign of the coefficient) at  $i = 90^\circ$  (fig. 23). Furthermore, since the odd zonal harmonics solely (to a first-order approximation) determine the long-period rate of change of the perilune altitude, selection of polar parking orbits may result in large  $\Delta V$  station-keeping requirements, dependent on the signs of the coefficients. If the signs of individual coefficients in the model are such that the  $\frac{de}{dt}$  rates reinforce each other, the  $\Delta V$  penalties might be substantial. Conversely, if the signs of the coefficients are such that the individual contributions interfere destructively, polar orbits may exist that have long lifetimes. This observation explains the discrepancy in the results shown in figure 7. For example, the signs of  $J_3$  and  $J_5$  for the Ferrari  $5 \times 5$

model are such that their eccentricity rates constructively interfere and yield short polar orbit lifetime predictions. Conversely, the sign and magnitude of the odd zonals for the Bills-Ferrari  $16 \times 16$  model allow the  $J_7$  term's large contribution to the eccentricity rate to effectively cancel out the contributions of the other terms. This superposition yields long-lifetime predictions for polar orbits.

## Concluding Remarks

Anticipation of future missions involving the placement of spacecraft in circular low-altitude parking orbits about the Moon for long periods of time motivated an investigation of the effects of the lunar gravitational field on an orbiting satellite. The formulation of a simplified five-coefficient lunar gravitational model was derived from Ferrari's  $5 \times 5$  gravitational model for the purpose of aiding mission planners in implementing nonspherical gravitational effects of the Moon in preliminary lunar mission studies. The proposed simplified gravitational model, consisting of the coefficients  $J_2$ ,  $J_3$ ,  $J_5$ ,  $C_{22}$ , and  $C_{31}$ , was adequate in predicting orbital lifetimes of lunar satellites; the results generated from its use closely corresponded to those generated by the Ferrari model. Furthermore, the simplified model reduced the amount of computer time required for lifetime predictions by approximately two orders of magnitude; this reduction greatly enhanced the capability to investigate the orbital lifetimes of lunar satellites as a function of the various initial orbital parameters.

Results generated with the Ferrari simplified five-coefficient gravitational model indicated the existence of several inclination bands of short-lifetime and long-lifetime orbits. These bands reflect the behavior of the perilune altitude decay rate that is associated with the  $J_5$  coefficient, the dominant term in the Ferrari model, as a function of inclination. Long orbital lifetimes were possible for low, midlatitude, and high-inclination orbits, although polar orbits had relatively short lifetimes (less than 180 days) according to this model. Of particular interest is the prediction of a narrow band of orbits with inclinations

between approximately  $60^\circ$  and  $75^\circ$  that yield high lifetimes while providing high-inclination orbits that are desirable for various missions. The lifetimes also depend on the initial value of argument of perilune, especially at low inclinations.

The  $C_{31}$  gravitational term generated dramatic localized effects in the behavior of orbital lifetimes, but did not contribute any secular effects to long-term predictions of lifetimes. The purely localized effects due to off-diagonal gravitational coefficients suggest that accurate long-term orbital predictions can be performed by consideration of only the zonal harmonics. Specifically, consideration of the odd zonal terms may be sufficient, as they have the primary influence on orbital-altitude secular decay rates. This technique provides a simple method to generate orbital lifetime predictions with other models.

Finally, the large uncertainty in the values of the coefficients for the Ferrari model (or any other lunar gravity model) indicates that little confidence can be placed in the results that are generated. In particular, the uncertainty in the value and even the sign of the  $J_5$  coefficient (a result of correlation between the  $J_3$  and the  $J_5$  term) contributes the dominant error associated with the Ferrari model. Current capabilities for long-term predictions of orbital lifetimes for lunar satellites leave much to be desired. However, the methods presented in this analysis are beneficial for incorporating the Moon's nonspherical gravitational effects on the preliminary design level for future lunar mission planning with little additional computational time required. Further work needs to be performed in the determination of an accurate lunar gravity model, as current models either give inconsistent predictions or predictions with such large uncertainty values that useful or meaningful interpretation of the results is difficult.

NASA Langley Research Center  
Hampton, VA 23681-0001  
November 15, 1993

Table 1. Numerical Values (Unnormalized) of Coefficients in Ferrari Model

[Boldface numbers denote values used in simplified model]

Degree	Order	$C_{nm} \times 10^4$	$S_{nm} \times 10^4$
2	0	<b>-2.0215</b>	
2	1	-0.001014	0
2	2	<b>0.22304</b>	0.000173
3	0	<b>-0.12126</b>	
3	1	<b>0.3071</b>	0.056107
3	2	0.048884	0.01687
3	3	0.01436	-0.0033435
4	0	0.0015	
4	1	-0.0718	0.0295
4	2	-0.01440	-0.02884
4	3	-0.00085	-0.00789
4	4	-0.001549	0.000564
5	0	<b>-0.446</b>	
5	1	-0.0326	0.0673
5	2	0.01556	-0.00522
5	3	-0.00148	0.00127
5	4	0.000598	0.000456
5	5	0.000122	0.000137

Table 2. Numerical Values (Unnormalized) of Coefficients in Bills-Ferrari Model

[From ref. 32]

Degree	Order	$C_{nm}$	$S_{nm}$
2	0	$-2.024 \times 10^{-4}$	
2	1	$-0.0904 \times 10^{-6}$	0
2	2	$0.2226 \times 10^{-4}$	$0.1936 \times 10^{-7}$
3	0	$-0.889 \times 10^{-5}$	
3	1	$0.2372 \times 10^{-4}$	$0.7160 \times 10^{-5}$
3	2	$0.0483 \times 10^{-4}$	$0.1626 \times 10^{-5}$
3	3	$0.2212 \times 10^{-5}$	$-0.3415 \times 10^{-4}$
4	0	$0.1173 \times 10^{-4}$	
4	1	$-0.4573 \times 10^{-5}$	$0.1812 \times 10^{-5}$
4	2	$-0.1818 \times 10^{-5}$	$-0.1512 \times 10^{-5}$
4	3	$0.2868 \times 10^{-7}$	$-0.8623 \times 10^{-6}$
4	4	$-0.7396 \times 10^{-7}$	$-0.1162 \times 10^{-7}$
5	0	$-0.2388 \times 10^{-5}$	
5	1	$-0.8272 \times 10^{-5}$	$-0.1310 \times 10^{-5}$
5	2	$0.6003 \times 10^{-6}$	$-0.3802 \times 10^{-6}$
5	3	$-0.1287 \times 10^{-7}$	$0.1622 \times 10^{-6}$
5	4	$0.4360 \times 10^{-8}$	$-0.5123 \times 10^{-7}$
5	5	$-0.1647 \times 10^{-7}$	$0.2856 \times 10^{-7}$
6	0	$0.1774 \times 10^{-4}$	
6	1	$0.9127 \times 10^{-6}$	$-0.5508 \times 10^{-7}$
6	2	$-0.5735 \times 10^{-6}$	$-0.4491 \times 10^{-6}$
6	3	$-0.4830 \times 10^{-7}$	$-0.8541 \times 10^{-7}$
6	4	$0.7759 \times 10^{-8}$	$-0.2914 \times 10^{-8}$
6	5	$0.2663 \times 10^{-8}$	$-0.6699 \times 10^{-8}$
6	6	$0.1824 \times 10^{-8}$	$-0.2227 \times 10^{-8}$
7	0	$0.2227 \times 10^{-4}$	
7	1	$0.1742 \times 10^{-5}$	$0.1632 \times 10^{-5}$
7	2	$-0.1753 \times 10^{-6}$	$-0.4582 \times 10^{-7}$
7	3	$-0.8736 \times 10^{-8}$	$0.1479 \times 10^{-7}$
7	4	$0.1890 \times 10^{-8}$	$0.7858 \times 10^{-9}$
7	5	$0.7750 \times 10^{-9}$	$0.3291 \times 10^{-9}$
7	6	$-0.1374 \times 10^{-9}$	$0.4588 \times 10^{-9}$
7	7	$-0.2059 \times 10^{-9}$	$0.1702 \times 10^{-9}$
8	0	$0.1493 \times 10^{-4}$	
8	1	$-0.7009 \times 10^{-6}$	$0.1752 \times 10^{-5}$
8	2	$0.1840 \times 10^{-6}$	$-0.4353 \times 10^{-7}$
8	3	$-0.7987 \times 10^{-8}$	$0.1688 \times 10^{-7}$
8	4	$0.588 \times 10^{-8}$	$-0.1436 \times 10^{-8}$
8	5	$-0.600 \times 10^{-9}$	$0.78 \times 10^{-9}$
8	6	$-0.111 \times 10^{-9}$	$-0.104 \times 10^{-9}$
8	7	$-0.153 \times 10^{-10}$	$-0.15 \times 10^{-11}$
8	8	$0.23 \times 10^{-11}$	$-0.97 \times 10^{-12}$

Table 3. Dominant Effects of Coefficients on Orbital Elements

[From ref. 3]

Coefficient	Principal orbital elements affected			
	Eccentricity	Node longitude	Argument of perilune	Inclination
$J_2$		•	•	
$J_3$	•			
$J_5$	•			
$C_{22}$				•
$C_{31}$	•		•	

## Appendix A

### First-Order Equations for Rates of Change of Orbital Elements

First-order equations for rates of change of the orbital elements due to  $J_2$ ,  $J_3$ ,  $J_5$ ,  $C_{22}$ , and  $C_{31}$  terms are as follows:

For  $J_2$ ,

$$\frac{da}{dt} = 0 \quad (\text{A1a})$$

$$\frac{de}{dt} = 0 \quad (\text{A1b})$$

$$\frac{di}{dt} = 0 \quad (\text{A1c})$$

$$\frac{d\Omega}{dt} = -\frac{3n}{2} \frac{R^2}{a^2(1-e^2)^2} J_2 \cos i \quad (\text{A1d})$$

$$\frac{d\omega}{dt} = \frac{3n}{4} \frac{R^2}{a^2(1-e^2)^2} J_2 (4 - 5 \sin^2 i) \quad (\text{A1e})$$

For  $J_3$ ,

$$\frac{da}{dt} = 0 \quad (\text{A2a})$$

$$\frac{de}{dt} = \frac{3n}{2} \frac{R^3}{a^3(1-e^2)^2} J_3 \sin i \left( \frac{5}{4} \sin^2 i - 1 \right) \cos \omega \quad (\text{A2b})$$

$$\frac{di}{dt} = -\frac{3n}{2} \frac{R^3 e}{a^3(1-e^2)^3} J_3 \cos i \left( \frac{5}{4} \sin^2 i - 1 \right) \cos \omega \quad (\text{A2c})$$

$$\frac{d\Omega}{dt} = -\frac{3n}{2} \frac{R^3 e}{a^3(1-e^2)^3} J_3 \cot i \left( \frac{15}{4} \sin^2 i - 1 \right) \sin \omega \quad (\text{A2d})$$

$$\frac{d\omega}{dt} = -\frac{3n}{2} \frac{R^3}{a^3(1-e^2)^3} J_3 \left[ \left( \frac{1+4e^2}{e} \right) \sin i \left( \frac{5}{4} \sin^2 i - 1 \right) - e \frac{\cos^2 i}{\sin i} \left( \frac{15}{4} \sin^2 i - 1 \right) \right] \sin \omega \quad (\text{A2e})$$

For  $J_5$ ,

$$\frac{da}{dt} = 0 \quad (\text{A3a})$$

$$\begin{aligned} \frac{de}{dt} = & \frac{15n}{8} \frac{R^5}{a^5(1-e^2)^4} J_5 \left[ \frac{7}{4} e^2 \sin^3 i \left( 1 - \frac{9}{8} \sin^2 i \right) \cos 3\omega \right. \\ & \left. + 2 \left( 1 + \frac{3}{4} e^2 \right) \sin i \left( \frac{21}{8} \sin^4 i - \frac{7}{2} \sin^2 i + 1 \right) \cos \omega \right] \end{aligned} \quad (\text{A3b})$$

$$\begin{aligned} \frac{di}{dt} &= \frac{15n}{8} \frac{R^5 e}{a^5 (1-e^2)^5} J_5 \left[ \frac{7}{4} e^2 \sin^2 i \cos i \left( \frac{9}{8} \sin^2 i - 1 \right) \cos 3\omega \right. \\ &\quad \left. - 2 \left( 1 + \frac{3}{4} e^2 \right) \cos i \left( \frac{21}{8} \sin^4 i - \frac{7}{2} \sin^2 i + 1 \right) \cos \omega \right] \end{aligned} \quad (\text{A3c})$$

$$\begin{aligned} \frac{d\Omega}{dt} &= \frac{15n}{8} \frac{R^5 e}{a^5 (1-e^2)^5} J_5 \left[ \frac{7}{4} e^2 \sin i \cos i \left( \frac{15}{8} \sin^2 i - 1 \right) \sin 3\omega \right. \\ &\quad \left. - 2 \left( 1 + \frac{3}{4} e^2 \right) \cot i \left( \frac{105}{8} \sin^4 i - \frac{21}{2} \sin^2 i + 1 \right) \sin \omega \right] \end{aligned} \quad (\text{A3d})$$

$$\begin{aligned} \frac{d\omega}{dt} &= \frac{15n}{8} \frac{R^5 e}{a^5 e (1-e^2)^5} J_5 \left\{ \frac{7}{4} e^2 \sin i \left[ \left( \frac{33}{8} e^2 + \frac{9}{8} \right) \sin^4 i + \left( -\frac{39}{8} e^2 - 1 \right) \sin^2 i + e^2 \right] \sin 3\omega \right. \\ &\quad \left. + \frac{2}{\sin i} \left[ \left( -\frac{693}{32} e^4 - \frac{1281}{32} e^2 - \frac{21}{8} \right) \sin^6 i + \left( \frac{1071}{32} e^4 + \frac{119}{2} e^2 + \frac{7}{2} \right) \sin^4 i \right. \right. \\ &\quad \left. \left. + \left( -\frac{105}{8} e^4 - \frac{87}{4} e^2 - 1 \right) \sin^2 i + \left( e^2 + \frac{3}{4} e^4 \right) \right] \sin \omega \right\} \end{aligned} \quad (\text{A3e})$$

For  $C_{22}$ ,

$$\frac{da}{dt} = 0 \quad (\text{A4a})$$

$$\frac{de}{dt} = 0 \quad (\text{A4b})$$

$$\frac{di}{dt} = \frac{3nR^2}{a^2(1-e^2)^2} C_{22} \sin i \sin 2\Omega_s \quad (\text{A4c})$$

$$\frac{d\Omega}{dt} = \frac{3nR^2}{a^2(1-e^2)^2} C_{22} \cos i \cos 2\Omega_s \quad (\text{A4d})$$

$$\frac{d\omega}{dt} = \frac{3n}{2} \frac{R^2}{a^2(1-e^2)^2} C_{22} \left( 5 \sin^2 i - 2 \right) \cos 2\Omega_s \quad (\text{A4e})$$

For  $C_{31}$ ,

$$\frac{da}{dt} = 0 \quad (\text{A5a})$$

$$\frac{de}{dt} = \frac{3n}{8} \frac{R^3}{a^3(1-e^2)^2} C_{31} \left[ \left( 5 \sin^2 i - 4 \right) \sin \omega \cos \Omega_s + \left( 15 \sin^2 i \cos i - 4 \cos i \right) \cos \omega \sin \Omega_s \right] \quad (\text{A5b})$$

$$\frac{di}{dt} = \frac{3n}{8} \frac{R^3 e}{a^3(1-e^2)^3} C_{31} \sin i \left[ 10 \cos i \sin \omega \cos \Omega_s + \left( 1 - 15 \cos^2 i \right) \cos \omega \sin \Omega_s \right] \quad (\text{A5c})$$

$$\frac{d\Omega}{dt} = -\frac{3n}{16} \frac{R^3 e}{a^3 (1-e^2)^3} C_{31} \left[ -20 \cos i \cos \omega \cos \Omega_s - (22 - 90 \cos^2 i) \sin \omega \sin \Omega_s \right] \quad (\text{A5d})$$

$$\begin{aligned} \frac{d\omega}{dt} = & -\frac{3n}{64} \frac{R^3 (1+4e^2)}{a^3 e (1-e^2)^3} C_{31} [(12 + 20 \cos 2i) \cos \omega \cos \Omega_s \\ & - (2 \cos i + 30 \cos 3i) \sin \omega \sin \Omega_s] - \left( \frac{d\Omega}{dt} \right)_{31} \cos i \end{aligned} \quad (\text{A5e})$$

where  $\left( \frac{d\Omega}{dt} \right)_{31}$  represents the  $\frac{d\Omega}{dt}$  contribution for the  $C_{31}$  term (eq. (A5d)). The  $\frac{d\Omega}{dt}$  term represents the rate of change in the inertial node longitude of the orbit  $\Omega$  referenced to the prime meridian at epoch (the prime meridian is defined by the Moon-Earth direction at some specified time). The selenographic node longitude of the orbit  $\Omega_s$  is related to the inertial node longitude by the expression  $\Omega_s = \Omega_i - \omega t$ . (See fig. A1.)

These equations (refs. 3 and 11) were in the computer program that was used to generate the plots for the three-dimensional and contour plots. They were also used in the sensitivity studies.

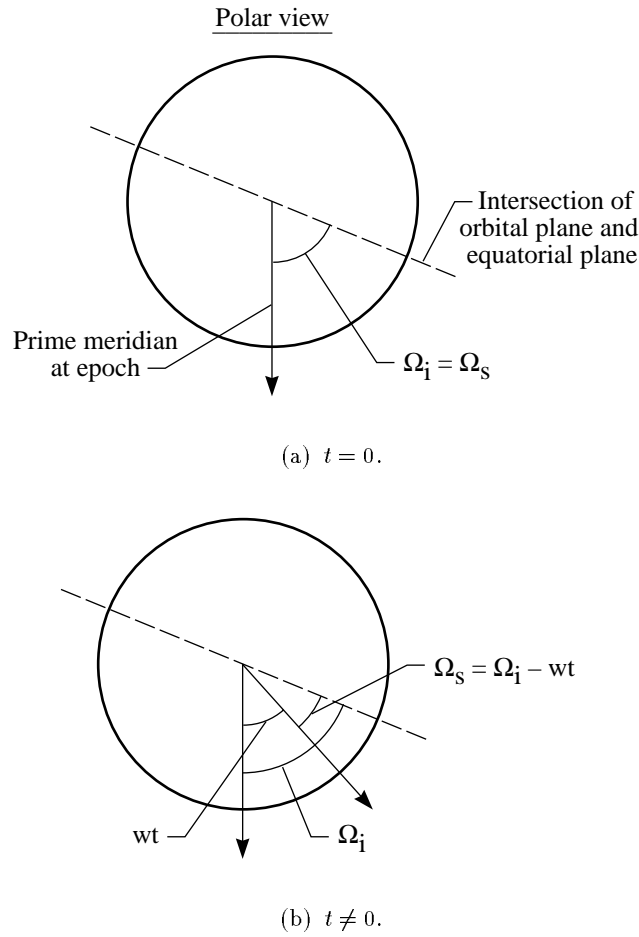


Figure A1. Differentiation between  $\Omega_i$  and  $\Omega_s$ .

## Appendix B

### Verification of Data Generated by Program LUNLIFE

The lunar lifetime program LUNLIFE<sup>1</sup> was originally intended to be the primary computational tool used in the present analysis. For this reason, much effort was invested in the verification of the data generated by this program. Although the development of the simplified gravitational model outlined in appendix C lessened the need for the use of the program LUNLIFE in this analysis, this program was essential for the formulation and verification of the simplified model. LUNLIFE was also used to quantify the effects due to solar radiation pressure (including shadowing effects) and Earth-Sun gravity perturbations (utilizing an analytical ephemeris algorithm). A direct descendant of software used in Viking mission studies, LUNLIFE numerically integrates the Lagrange planetary equations of motion (eqs. (4)) with a fixed-interval fourth-order predictor-corrector algorithm, and addresses perturbations through the use of disturbing functions developed by Kaula. (See refs. 40 and 41.)

LUNLIFE was initially tested by comparing it to results contained in a Boeing report on a lunar model for Apollo. (See ref. 3.) The model in the Boeing report was ideal for comparison since it consisted of only four gravitational coefficients. A list of first-order analytical equations in the appendix of the Boeing report also allowed for testing of the effects of individual gravitational coefficients on each of the orbital elements. Results generated by the Goddard Space Flight Center in the 1970's for a lunar lifetime study (ref. 4) were also duplicated with LUNLIFE.

In this study, three  $3 \times 3$  lunar gravity models were used to specifically address satellite lifetimes in near polar orbits.

Additionally, LUNLIFE was compared in figure B1 with the computer programs ASAP (ref. 39) and LUNNODE<sup>1</sup>. These two programs differ from LUNLIFE in that they integrate the equations of motion in Cartesian coordinates. As a result, much smaller time steps are used, and the programs include short-period effects rather than averaging them out. The comparisons were made with an  $8 \times 8$  truncated version of the Bills-Ferrari  $16 \times 16$  gravitational model. (See ref. 32.) The three programs generated near-identical data of perilune altitude versus time. The various sources have validated the data that was generated by LUNLIFE and have verified the results that were generated by the method introduced in appendix C.

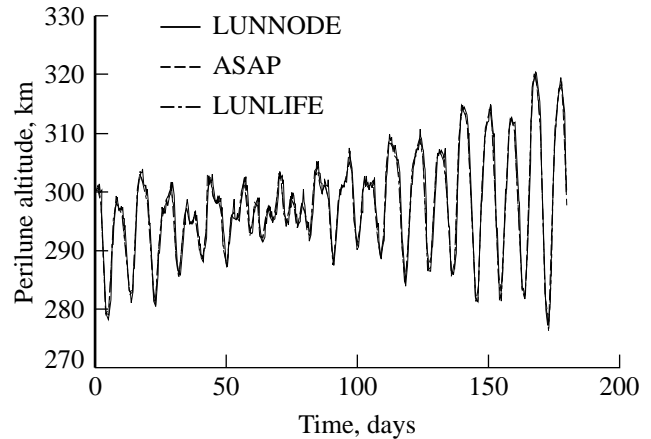


Figure B1. Verification of results generated by program LUNLIFE.

<sup>1</sup> Developed by Flight Mechanics & Control under NASA contract NAS1-18267 in February 1989.

## Appendix C

### Comparison of Simplified Gravity Model With Ferrari $5 \times 5$ Model

The formulation of a simplified five-coefficient lunar gravitational model was derived from Ferrari's  $5 \times 5$  gravitational model for the purpose of aiding mission planners in implementing nonspherical gravitational effects of the Moon in preliminary lunar mission studies. The proposed simplified gravitational model consisted of the coefficients  $J_2$ ,  $J_3$ ,  $J_5$ ,  $C_{22}$ , and  $C_{31}$ . Several cases were analyzed with various initial orbital parameters to examine the changes in perilune altitude, longitude of ascending node, and argument of perilune between the Ferrari  $5 \times 5$  model and the simplified five-coefficient gravity model.

A wide range of cases were analyzed by varying the initial inclination, longitude of ascending node, and argument of perilune. The initial mean anomaly was set to zero, the initial eccentricity was fixed at 0.05 (for consideration of near-circular orbits), and the semimajor axis value of 1935.79 km was selected to yield an initial perilune altitude of 100 km. Initial inclination values of  $1^\circ$ ,  $45^\circ$ ,  $90^\circ$ ,  $120^\circ$ ,  $150^\circ$ , and  $179^\circ$  were selected to simulate both posigrade and retrograde orbits. In an effort to cover different quadrants, since  $\cos \omega$  and  $\sin \omega$  appear in the analytical expressions derived from the Lagrange planetary equations, initial values of argument of perilune selected were  $0^\circ$ ,  $135^\circ$ , and  $225^\circ$ . Initial values of longitude of ascending node of  $0^\circ$ ,  $135^\circ$ , and  $225^\circ$  were chosen for the same reasons. The presence of sectorial and tesseral harmonic coefficients in the lunar models introduces a longitudinal dependence in the gravitational potential. This dependence makes it necessary to utilize several different initial values for longitude of ascending node. If only zonal harmonic coefficients were included in the models, results would be independent of initial values of longitude of ascending node. Exhausting all combinations of the values, 54 different initial conditions were analyzed. Each case was evaluated for both the Ferrari  $5 \times 5$  model and the simplified five-coefficient lunar gravity model.

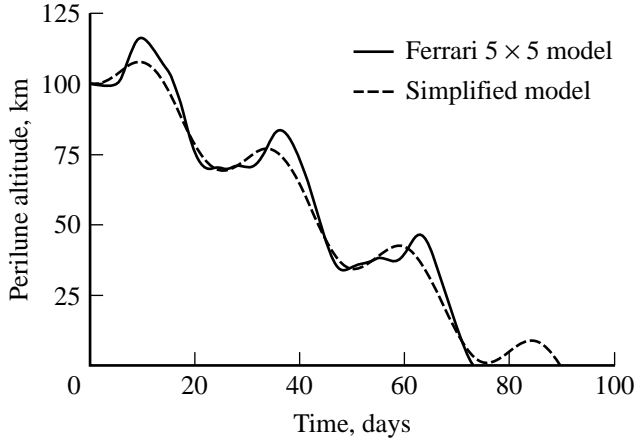
A single simplified gravitational model was presumed to be insufficient for accurate orbital predictions over all inclinations, because the magnitude of the effects contributed by each individual gravitational coefficient is a function of inclination. However, the simple model did make accurate predictions over all latitudes that were tested. The results of the Ferrari  $5 \times 5$  model and the simplified model were analyzed by comparing their orbital lifetimes

if they were less than 180 days. If the lifetimes exceeded 180 days (calculations were terminated after 180 days), the two models were analyzed by comparing their minimum perilune-altitude values during this time period. Lifetimes were the shortest for inclinations of  $90^\circ$  and  $120^\circ$ , as each trial that was examined resulted in impact with the lunar surface in less than 180 days. Near-equatorial orbits ( $1^\circ$ ,  $179^\circ$ ) had the smallest decrease in perilune altitude; each case examined had lifetimes in excess of 180 days. These results are listed in table C1.

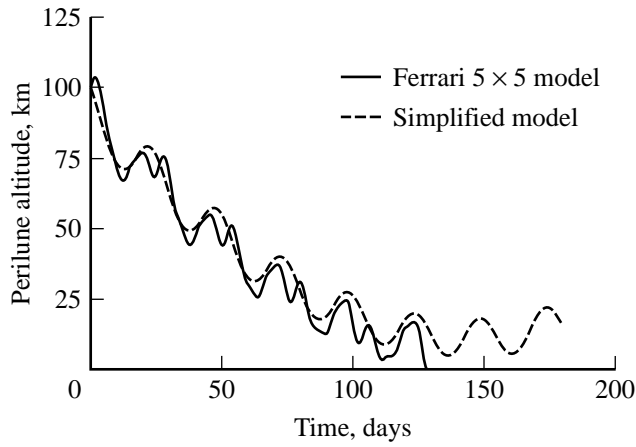
The data generated with the simplified five-coefficient model matched very closely the data generated with the Ferrari  $5 \times 5$  model. For cases with lifetimes of less than 180 days, the simplified model usually predicted the lifetimes within 4 days of the Ferrari model. For cases with lifetimes longer than 180 days, the simplified model usually predicted the minimum perilune altitude within 10 km of the Ferrari model. There is no particular inclination range where the two gravitational models seem to be in better agreement. Also, the simplified model does not consistently overestimate or underestimate the orbital lifetimes compared with the Ferrari model.

There were two cases for which the difference in predictions of the orbital lifetimes was significant. In the first case ( $i = 45^\circ$ ,  $\Omega = 135^\circ$ ,  $\omega = 135^\circ$ ), the simplified model underestimated the lifetime by 16 days. (See fig. C1(a).) The simplified model slightly underpredicted the rate of decay of the perilune altitude through 74 days. This underprediction allowed the satellite to temporarily avoid a collision and, with the assistance of the medium-period effects, enabled the orbit to survive for an additional 16 days. In the second case ( $i = 45^\circ$ ,  $\Omega = 0^\circ$ ,  $\omega = 225^\circ$ ), the Ferrari model predicted an orbital lifetime of 129 days; the simplified model predicted a lifetime in excess of 180 days, with a minimum perilune altitude of 5 km for the first 180 days. (See fig. C1(b).) The explanation for this discrepancy is that the simplified model again underpredicted the rate of perilune decay, allowing the orbit to exist past 129 days, and, with the assistance of the long-period effects, enabled the perilune altitude to actually increase. These two cases do not hinder the usefulness of the simplified model, as both of the discrepancies can be eliminated by assigning a small margin of error (around 5 km) to the value of the perilune altitude predicted by the simplified model.

Also, the longitude of ascending node and argument of perilune were monitored in this analysis. These orbital element values (computed with the simplified and Ferrari models) also compared well, although not quite as well as the perilune-altitude



(a) Initial conditions:  $i = 45^\circ$ ,  $\Omega = 135^\circ$ ,  $\omega = 135^\circ$ .



(b) Initial conditions:  $i = 45^\circ$ ,  $\Omega = 0^\circ$ ,  $\omega = 225^\circ$ .

Figure C1. Comparison of perilune altitude for simplified and Ferrari models.

predictions. The longitude of ascending node precession was consistent between the two models, since the  $J_2$  term, which is the dominant term for determining

nodal precession, is included in both models. Agreement of the argument of perilune was not always as promising, since near-circular orbits are addressed in this analysis. For near-circular orbits (where a unique  $\omega$  is not defined), large changes in the argument of perilune often take place, these changes tend to amplify any differences between the two models.

In the present analysis, the simplified gravitational model generated results similar to those of the Ferrari model for initial altitudes of 100 km. Verification of accuracy for other initial altitudes would increase the applicability of this model. The simplified model proposed in this analysis might be further improved by directly mapping the observational data to the five coefficients, as opposed to the present method (a truncated version of the Ferrari model) of adopting the values of the coefficients directly from the Ferrari model.

This analysis suggests that other simplified gravitational models could be proposed to simulate even higher order models for the purpose of generating orbital lifetime predictions without sacrificing accurate results. However, the capability of the proposed model to duplicate results similar to the Ferrari model has not yet been verified for other initial perilune altitudes, and the proposed model is not expected to generate results similar to those predicted by other gravitational models. Since other models differ in the magnitude (and perhaps even sign) of their coefficients, a selection of coefficients other than the ones stated in the proposed simplified model presented herein may be more appropriate for simulating the results of that particular model. Also, models with a larger number of gravitational terms may be more difficult to simulate with a simplified model because of the magnitude of the contribution of the higher order terms.

Table C1. Comparison of Orbital Lifetimes

(a)  $i = 1^\circ, 45^\circ,$  and  $90^\circ$ 

Initial orbital elements			Ferrari $5 \times 5$ model		Simplified model	
$i,$ deg	$\Omega,$ deg	$\omega,$ deg	Orbital lifetime, <sup>a</sup> days	Minimum altitude, km	Orbital lifetime, <sup>a</sup> days	Minimum altitude, km
1	0	0		42		54
1	0	135		95		92
1	0	225		78		87
1	135	0		89		88
1	135	135		60		78
1	135	225		39		54
1	225	0		84		88
1	225	135		45		56
1	225	225		73		72
45	0	0		22		25
45	0	135	62		65	
45	0	225	129			5
45	135	0		16		13
45	135	135	74		90	
45	135	225		10		16
45	225	0		13		3
45	225	135	78		76	
45	225	225		18		10
90	0	0	47		47	
90	0	135	102		99	
90	0	225	144		145	
90	135	0	45		48	
90	135	135	97		97	
90	135	225	139		141	
90	225	0	52		48	
90	225	135	105		101	
90	225	225	147		143	

<sup>a</sup>Orbital lifetime if  $< 180$  days.

Table C1. Concluded

(b)  $i = 120^\circ, 150^\circ, \text{ and } 179^\circ$ 

Initial orbital elements			Ferrari $5 \times 5$ model		Simplified model	
$i$ , deg	$\Omega$ , deg	$\omega$ , deg	Orbital lifetime, <sup>a</sup> days	Minimum altitude, km	Orbital lifetime, <sup>a</sup> days	Minimum altitude, km
120	0	0	167		167	
120	0	135	77		77	
120	0	225	77		78	
120	135	0	149		(b)	
120	135	135	59		59	
120	135	225	60		59	
120	225	0	154		148	
120	225	135	44		44	
120	225	225	44		46	
150	0	0		5		10
150	0	135		77		75
150	0	225	136		133	
150	135	0		11		4
150	135	135		46		61
150	135	225	114		114	
150	225	0		19		15
150	225	135		80		75
150	225	225	127		126	
179	0	0		95		96
179	0	135		66		59
179	0	225		51		63
179	135	0		53		64
179	135	135		99		99
179	135	225		74		74
179	225	0		61		65
179	225	135		71		79
179	225	225		95		94

<sup>a</sup>Orbital lifetime if  $< 180$  days.<sup>b</sup>Singularity in model caused erroneous prediction.

## References

1. Alred, John; Bufkin, Ann; Kennedy, Kriss J.; Petro, Andrew; Roberts, Michael; Stecklein, Jonette; and Sturm, James: *Lunar Outpost*. JSC-23613, NASA Lyndon B. Johnson Space Center, 1989.
2. Synthesis Group on America's Space Exploration Initiative: *America at the Threshdd*. U.S. Government Printing Off., 1991.
3. Risdal, R. E.: *Development of a Simple Lunar Model for Apollo—Final Report*. NASA CR-66760, 1969.
4. Kwok, J. M.: *Comparison of Lunar Gravity Models and Calibration of the Numerical Averaging Method for Lifetime Prediction of the Lunar Polar Orbiter*. 3000-28400-01TM (Contract No. NAS5-11999, Task Assignment No. 284), Computer Sciences Corp., 1979.
5. Cook, Richard A.; Sergeevsky, Andrey B.; Belbruno, Edward A.; and Sweetser, Theodore H.: Return to the Moon—The Lunar Observer Mission. A Collection of Technical Papers, Part 1—AIAA/AAS Astrodynamics Conference, Aug. 1990, pp. 232–245. (Available as AIAA-90-2888.)
6. Guttman, Peter T.: Lifetime of a Lunar Orbit Space Station (LOSS). AAS Paper 71-377, Aug. 1971.
7. Menzel, Donald H.: *Mathematical Physics*. Dover Publ., Inc., 1961.
8. Heiskanen, Weikko A.; and Moritz, Helmut: *Physical Geodesy*. W. H. Freeman & Co., 1967.
9. Wells, William R.: Notes on Gravitational Potential Theory. Eng. Ext. Ser. Circ. No. 6, Virginia Polytechnic Inst., [1966].
10. Kaula, William M.: *An Introduction to Planetary Physics—The Terrestrial Planets*. John Wiley & Sons, Inc., 1968.
11. Merson, R. H.: The Motion of a Satellite in an Axisymmetric Gravitational Field. *Geophys. J.*, vol. 4, 1961, pp. 17–52.
12. Sagitov, M. U.: *Lunar Gravimetry*. FTD-ID(RS)T-0645-84, U.S. Air Force, Sept. 1985. (Available from DTIC as AD B095 274.)
13. Muller, P. M.; and Sjogren, W. L.: Mascons: Lunar Mass Concentrations. *Science*, vol. 161, no. 3842, Aug. 16, 1968, pp. 680–684.
14. Phillips, R. J.; Conel, J. E.; Abbott, E. A.; Sjogren, W. L.; and Morton, J. B.: Mascons—Progress Toward a Unique Solution for Mass Distribution. *J. Geophys. Res.*, vol. 77, no. 35, Dec. 10, 1973, pp. 7106–7114.
15. Ananda, Mohan P.: Lunar Gravity—A Mass Point Model. *J. Geophys. Res.*, vol. 82, no. 20, July 1977, pp. 3049–3064.
16. Wong, L.; Buechler, G.; Downs, W.; Sjogren, W.; Muller, P.; and Gottlieb, P.: A Surface-Layer Representation of the Lunar Gravitational Field. *J. Geophys. Res.*, vol. 76, no. 26, Sept. 1971, pp. 6220–6236.
17. Smith, D. E.: *First Order Perturbations of an Orbit by a Mass Anomaly*. NASA TM X-63921, 1970.
18. Ananda, Mohan: Mean Rates of the Orbital Elements of a Satellite Perturbed by a Lens Shaped Mass Concentration. *Celest. Mech.*, vol. 12, Dec. 1975, pp. 495–511.
19. Salama, Ahmed H.: An Analytical Evaluation of Mascon Effects in a Semi-Analytic Theory. *Astrodynamics 1991—Proceedings of the AAS/AIAA Astrodynamics Conf.*, Part 3, Univelt, Inc., 1992, pp. 2173–2189. (Available as AAS Paper 91-461.)
20. Kaplan, Marshall H.; and Kunciw, Bohdan G.: Lunar Gravity Model Obtained by Using Spherical Harmonics With Mascon Terms. *The Use of Artificial Satellites for Geodesy*, Soren W. Henriksen, Armando Mancini, and Bernard H. Chovitz, eds., Geophys. Monogr. 15, American Geophysical Union, 1972, pp. 265–273.
21. Buglia, James J.: *Compilation of Methods in Orbital Mechanics and Solar Geometry*. NASA RP-1204, 1988.
22. Desai, Prasun N.; Braun, Robert D.; and Powell, Richard W.: *Aspects of Parking Orbit Selection in a Manned Mars Mission*. NASA TP-3256, 1992.
23. Ferrari, A. J.; Sinclair, W. S.; Sjogren, W. L.; Williams, J. G.; and Yoder, C. F.: Geophysical Parameters of the Earth-Moon System. *J. Geophys. Res.*, vol. 85, no. B7, July 1980, pp. 3939–3951.
24. Ferrari, A. J.; and Heffron, W. G.: Effects of Physical Librations of the Moon on the Orbital Elements of a Lunar Satellite. *Celest. Mech.*, vol. 8, Aug. 1973, pp. 111–120.
25. Michael, William H., Jr.; and Blackshear, W. Thomas: Recent Results on the Mass, Gravitational Field and Moments of Inertia of the Moon. *Moon*, vol. 3, Mar. 1972, pp. 388–402.
26. Ferrari, Alfred J.: Lunar Gravity—A Harmonic Analysis. *J. Geophys. Res.*, vol. 82, no. 20, July 1977, pp. 3065–3084.
27. Gapcynski, J. P.; Blackshear, W. T.; Tolson, R. H.; and Compton, H. R.: A Determination of the Lunar Moment of Inertia. *Geophys. Res. Lett.*, vol. 2, no. 8, Aug. 1975, pp. 353–356.
28. Branley, Franklyn Mansfield: *The Moon, Earth's Natural Satellite*. Crowell, 1960. (Available as SYNC04-1.)
29. Kaula, William M.: The Gravity and Shape of the Moon. *EOS Trans., American Geophys. Union*, vol. 56, no. 6, June 1975, pp. 309–316.
30. Cook, Richard A.: *Orbit Design for Lunar Missions*. Eng. Memo. 312-90/160, Jet Propulsion Lab., June 1990.
31. Laing, P. A.; Liu, A. S.: Lunar Gravity Analysis From Long-Term Effects. *Science*, vol. 173, 1971, pp. 1017–1020.
32. Bills, Bruce G.; and Ferrari, Alfred J.: A Harmonic Analysis of Lunar Gravity. *J. Geophys. Res.*, vol. 85, no. B2, Feb. 1980, pp. 1013–1025.

33. Akim, E. L.; and Vlasova, Z. P.: Investigation of the Lunar Gravitational Field According to Measurements of the Trajectories of Soviet Artificial Lunar Satellites. *Kosmicheskie Issledovaniia* (Russian), vol. 21, 1983, pp. 499–511.
34. Sagitov, M. U.: Lunar Gravimetry. FTD-ID(RS)T-0645-84, U.S. Air Force, Sept. 1985.
35. Cook, Richard A.; and Sweetser, Theodore H.: Orbit Maintenance for Low Altitude Near-Circular Lunar Orbits. AAS Paper 92-185, Feb. 1992.
36. Lorell, J.: *Application of Double-Averaged Equations of Satellite Motion to a Lunar Orbiter*. NASA CR-76200, 1966.
37. Williams, R. R.; and Lorell, J.: *The Theory of Long-Term Behavior of Artificial Satellite Orbits Due to Third-Body Perturbations*. NASA CR-70738, 1966.
38. Battin, Richard H.: *An Introduction to the Mathematics and Methods of Astrodynamics*. American Inst. of Aeronautics and Astronautics, Inc., 1987.
39. Kwok, Johnny H.: *The Artificial Satellite Analysis Program (ASAP), Volume 2.0*. NPO-17522, COSMIC, Univ. of Georgia, 1987.
40. Kaula, William M.: *Theory of Satellite Geodesy: Applications of Satellites to Geodesy*. Blaisdell Publ. Co., 1966.
41. Kaula, William M.: Development of the Lunar and Solar Disturbing Functions for a Close Satellite. *Astron. J.*, vol. 67, no. 5, June 1962, pp. 300–303.

REPORT DOCUMENTATION PAGE			Form Approved OMB No. 0704-0188	
Public reporting burden for this collection of information is estimated to average 1 hour per response, including the time for reviewing instructions, searching existing data sources, gathering and maintaining the data needed, and completing and reviewing the collection of information. Send comments regarding this burden estimate or any other aspect of this collection of information, including suggestions for reducing this burden, to Washington Headquarters Services, Directorate for Information Operations and Reports, 1215 Jefferson Davis Highway, Suite 1204, Arlington, VA 22202-4302, and to the Office of Management and Budget, Paperwork Reduction Project (0704-0188), Washington, DC 20503.				
1. AGENCY USE ONLY (Leave blank)	2. REPORT DATE March 1994	3. REPORT TYPE AND DATES COVERED Technical Paper		
4. TITLE AND SUBTITLE Lifetimes of Lunar Satellite Orbits			5. FUNDING NUMBERS WU 506-49-11-01	
6. AUTHOR(S) Kurt W. Meyer, James J. Buglia, and Prasun N. Desai				
7. PERFORMING ORGANIZATION NAME(S) AND ADDRESS(ES) NASA Langley Research Center Hampton, VA 23681-0001			8. PERFORMING ORGANIZATION REPORT NUMBER L-17264	
9. SPONSORING/MONITORING AGENCY NAME(S) AND ADDRESS(ES) National Aeronautics and Space Administration Washington, DC 20546-0001			10. SPONSORING/MONITORING AGENCY REPORT NUMBER NASA TP-3394	
11. SUPPLEMENTARY NOTES Meyer: The George Washington Univ., JIAFS, Langley Research Center, Hampton, VA; Buglia: Flight Mechanics & Control, Inc., Hampton, VA; Desai: Langley Research Center, Hampton, VA. The majority of this research was performed by Kurt W. Meyer in partial fulfillment of a Master of Science degree at The George Washington University.				
12a. DISTRIBUTION/AVAILABILITY STATEMENT  Unclassified-Unlimited  Subject Category 13			12b. DISTRIBUTION CODE	
13. ABSTRACT (Maximum 200 words) The Space Exploration Initiative has generated a renewed interest in lunar mission planning. The lunar missions currently under study, unlike the Apollo missions, involve long stay times. Several lunar gravity models have been formulated, but mission planners do not have enough confidence in the proposed models to conduct detailed studies of missions with long stay times. In this report, a particular lunar gravitational model (the Ferrari 5 x 5 model) was chosen to determine the lifetimes for 100-km and 300-km perilune altitude, near-circular parking orbits. The need to analyze orbital lifetimes for a large number of initial orbital parameters was the motivation for the formulation of a simplified gravitational model from the original model. Using this model, orbital lifetimes were found to be heavily dependent on the initial conditions of the nearly circular orbits, particularly the initial inclination and argument of perilune. This selected model yielded lifetime predictions of less than 40 days for some orbits, and other orbits had lifetimes exceeding a year. Although inconsistencies and limitations are inherent in all existing lunar gravity models (primarily because of a lack of information about the far side of the Moon), the methods presented in this analysis are suitable for incorporating the Moon's nonspherical gravitational effects on the preliminary design level for future lunar mission planning.				
14. SUBJECT TERMS Lunar parking orbits; Lunar missions; Lunar orbit lifetimes; Lunar nonspherical gravitational effects			15. NUMBER OF PAGES 36	
			16. PRICE CODE A03	
17. SECURITY CLASSIFICATION OF REPORT Unclassified	18. SECURITY CLASSIFICATION OF THIS PAGE Unclassified	19. SECURITY CLASSIFICATION OF ABSTRACT	20. LIMITATION OF ABSTRACT	